Mathematical Medicine and Biology: A Journal of the IMA (2022) **39**, 332–367
https://doi.org/10.1093/imammb/dqac009
Advance Access publication on 21 June 2022

Multi-scale modelling of nanoparticle delivery and heat transport in vascularised tumours

Tahani Al Sariri
School of Mathematics and Statistics, University of Glasgow, University Place, Glasgow, G12 8QQ, UK,
Department of Mathematics, College of Science, Sultan Qaboos University, Al-Khoudh 123, Oman

and

Raimondo Penta*
School of Mathematics and Statistics, University of Glasgow, University Place, Glasgow, G12 8QQ, UK
*Corresponding author. Email: Raimondo.Penta@glasgow.ac.uk

[Received on 6 May 2021; revised on 11 May 2022; accepted on 9 June 2022]

We focus on modelling of cancer hyperthermia driven by the application of the magnetic field to iron oxide nanoparticles. We assume that the particles are interacting with the tumour environment by extravasating from the vessels into the interstitial space. We start from Darcy's and Stokes' problems in the interstitial and fluid vessels compartments. Advection–diffusion of nanoparticles takes place in both compartments (as well as uptake in the tumour interstitium), and a heat source proportional to the concentration of nanoparticles drives heat diffusion and convection in the system. The system under consideration is intrinsically multi-scale. The distance between adjacent vessels (the *micro-scale*) is much smaller than the average tumour size (the *macro-scale*). We then apply the asymptotic homogenisation technique to retain the influence of the micro-structure on the tissue scale distribution of heat and particles. We derive a new system of homogenised partial differential equations (PDEs) describing blood transport, delivery of nanoparticles and heat transport. The new model comprises a double Darcy's law, coupled with two double advection–diffusion–reaction systems of PDEs describing fluid, particles and heat transport and mass, drug and heat exchange. The role of the micro-structure is encoded in the coefficients of the model, which are to be computed solving appropriate periodic problems. We show that the heat distribution is impaired by increasing vessels' tortuosity and that regularization of the micro-vessels can produce a significant increase (1–2 degrees) in the maximum temperature. We quantify the impact of modifying the properties of the magnetic field depending on the vessels' tortuosity.

Keywords: hyperthermia cancer treatment; nanoparticle delivery; homogenisation; heat convection; Vessels' tortuosity.

1. Introduction

Tumours are cancerous tissues consisting of different cells that interact with each other by heterotypic interaction i.e. involving both cancerous and non-cancerous cells and constituents. They are characterized by different hallmarks that enable them to develop and growth in the body. The cancer cells preserve the chronic proliferative signals and avoid the suppressor genes, which regulate cell duplication. While normal cells replication is limited, cancer cells can grow in an uncontrolled way thus producing the tumour mass. In addition, tumours are capable of obtaining nutrients and oxygen from the angiogenic

microvasculature. Subsequently, the malignant cells spread in different parts of the body, as reported by Hanahan & Weinberg (2011).

Healthy vessels greatly differ from the malignant ones. In fact, these latter are well known to be less organized, more tortuous and dilated, with highly permeable walls characterized by openings and geometrical defects, as reported e.g. by Hashizume *et al.* (2000). Enhancing drug transport in tumours plays a prominent role in improving anti-cancer therapies. The disorganized vascular network increases the interstitial fluid pressure (IFP), which leads to a reduced fluid convection, and, in turn, impaired drug transport within the tumour mass, see, e.g. the work by Jain *et al.* (2007). Higher levels of IFP are due to the leaky tumour vessels that are unable to preserve the oncotic and hydrostatic pressure gradients across the vessel walls. In the manuscript by Jain *et al.* (2007), the authors have studied the effect of antiangiogenic therapy to increase the fluid convection inside the tumour and decrease the convection outside the tumour by reducing the IFP. This can for instance be achieved by decreasing tumour size and permeability of the vessels' wall, surface area of the tumour vessels, and increasing the hydraulic conductivity. More recently, Penta & Ambrosi (2015) have shown that geometrical regularization of the microvessels can likewise play a key role in improving fluid and drug convection within the tumours mass.

Hyperthermia treatment and thermal ablation are emerging strategies for treating cancer. Hyperthermia is typically used to indicate treatments where the malignant cell is exposed to an heat source until the temperature exceeds a given target (this is typically around 42 °C). It typically takes a long time to reach the target temperature, so this strategy is normally supplemented by other treatments such as chemotherapy and radiation in order to have a significant decline in the tumour size. The extreme case of hyperthermia treatment is usually referred to as thermal ablation. In this latter case, the temperature can reach up to approximately 50 °C in a shorter period of time. However, this strategy has limitations in reaching a complete eradication of the tumour cells, which is likely to cause the cancer recurrence, as reported by Cervadoro *et al.* (2013).

In the past few decades, the use of nanoparticles has been increasingly embraced to develop drug delivery (see, e.g., the work by Singh *et al.* (2011)), because of their chemical and physical properties. Nanoparticles possess peculiar characteristics related to their sizes and surfaces, which enable them to remain in the blood without causing any toxicity. The so called iron oxide nanoparticles (IONP) and gold nanoparticles (AuNP) are examples of drug delivery vectors which are used to carry out hyperthermia treatments. On the one hand, AuNPs generate heat after absorbing the near-infra red (nIR), but this wavelength has limitation on the tumour depth that can be reached. Therefore, this strategy might not be efficient to kill malignant cells uniformly. On the other hand, the temperature increase obtained by using IONP is related to the application of an external magnetic field. IONP are transported to the tumour via two distinct mechanisms: *passive* and *active*. Passive means that the particles are transported to the tumour through the capillaries by diffusion or convection. In the active case, the particles bind with the tumour receptors and are metabolized, as illustrated e.g. by Martinkova *et al.* (2018). The magnetic field is applied when the particles reach the tumour. The magnetic energy is then converted into thermal energy as described by the Brownian Neel relaxation equation, see e.g. the work by Kaddi *et al.* (2013).

In this work we aim to describe the temperature maps related to hyperthermia cancer treatment performed via IONPs transported by means of the passive mechanisms (i.e. the formulation is applicable to particles that are sufficiently small to extravasate from the vessels to the tumour). We account for the three-dimensional character of both the tumour and the vessels, which are considered as two interacting domains as done by Mascheroni & Penta (2017); Penta & Ambrosi (2015). In the latter papers, the authors found that the vessels' tortuosity impaired the fluid and macromolecules drug flow in vascularised tumours. In this work we extend their results to cover the influence of geometrical tortuosity on heat transport in the context of cancer hyperthermia. The vessels' fluid flow is governed

by the Stokes' problem, while we assume that interstitial transport is described by Darcy's law. The governing equations describing drug transport are of advection–diffusion type in the vessels and of advection–diffusion–reaction type in the tumour interstitium. Diffusive and advective heat transport in both compartments is likewise formally represented by a double advection–diffusion–reaction model. The vessel's wall is modeled as a porous semi-permeable membrane, so as to allow the interplay of fluid, mass, and heat between compartments.

In this work we address the sharp length scale that exists between the typical intercapillary distance and the average tumour size by means of the asymptotic homogenisation technique, as summarized e.g. in the works by Bakhvalov & Panasenko (1989); Cioranescu & Donato (1999); Davit *et al.* (2013); Taffetani *et al.* (2014); Penta & Gerisch (2017). This strategy provides the upscaled parameters at the macro-scale on the basis of the micro-scale geometry and structural properties. In particular, the resulting macro-scale governing equations encode the crucial role of the micro-scale structure in the coefficient of the model. This approach is motivated by the fact that real-world problems typically involve interactions between a variety of physical three-dimensional systems characterized by different properties. In general, it is practically impossible to resolve all the micro-scale details in three dimensions. Furthermore, experiment measurements are typically performed at the macro-scale. This method has been successfully applied to several scenarios, including heterogeneous porous media, as shown by Penta *et al.* (2021), vascularised tumours, as in the manuscript by Shipley & Chapman (2010); Penta *et al.* (2015), and biofilms, e.g. as illustrated by Dalwadi & King (2020).

Our macro-scale results comprise a double Darcy's system of partial differential equations (PDEs) describing fluid transport within and between compartments, and double advection–diffusion–reaction equations for both drug and heat transport. The influence of the micro-structure appears in the hydraulic conductivities, particle diffusion coefficients and thermal conductivities, which can be determined by solving appropriate periodic cell problems. The macro-scale system of PDEs is solved by finite elements in a spherical coordinate setting. The results elucidate the role of tortuosity and absorption rate, as well as their mutual interplay, on heat transport generated by nanoparticles in vascularised tumours.

Nabil & Zunino (2016) discussed the hyperthermia cancer treatment using IONP by primarily focussing on the adhesion mechanisms (so that excited particles do not extravasate from the vessels to the tumour). However, this work is different from the one by Nabil & Zunino (2016) as here the tumour is modeled as a three-dimensional domain, which comprises the interstitial spaces and the vessels. The two domains are separated by an interface that represents the vessels' walls. Moreover, there are some differences between the two works related to the macro-scale geometry, computational technique and other concepts such as external boundary conditions. For instance, Nabil & Zunino (2016) represent the tumour at the macro-scale as a cube for the sake of simplifying the numerical computations. In contrast, we modelled the vascularised tumour as a sphere as an analogy with the works by Penta *et al.* (2015); Penta & Ambrosi (2015); Shipley & Chapman (2010). This geometry has significant implications on the fluid and drug transport profile and also this particular shape is very convenient when comparing results against experiments, as shown by Jain & Baxter (1988). In addition, the homogenisation technique adopted by Nabil & Zunino (2016) relies on the *immersed boundary method*, as illustrated by Cattaneo & Zunino (2014a,b). The vessels are dealt with as though they were one-dimensional lines, nevertheless carrying relevant three-dimensional information via appropriate singularities on the boundaries. Our new model retained the three-dimensional character of both the vessels and the interstitial spaces, and asymptotic homogenisation is being used to perform the upscaling and achieve computational feasibility. In this way, the geometrical differences between the vessels and tumour are smoothed out on the macro-scale. Moreover, in the present work, we encode information related to the fine-scale structure of the individual compartments, as well as the transport that is occurring across the vessels' walls. The latter

is reflected into appropriate sources at the macroscopic scale. In the work by Nabil & Zunino (2016), the interface is not resolved as the vessels are immersed in the three dimensional tumour. However, in their case, information concerning fluid, drug and heat transport across the interface is retained and it appears likewise as a source in the resulting macro-scale model. Furthermore, the vessels temperature is constant in their work, but it varies in our work, as the vessels are represented by a separate compartment in three dimensions, which is described by its own governing equations. In addition, Nabil & Zunino (2016) consider different time steps that depend on the size of nanoparticles. A 40 minutes time interval appropriate for very small nanoparticles and 12 h, 24 h and 48 h for large ones that are called vascular magnetic nanoparticles. In our case, we do not focus on the size of nanoparticles and we focus on a 4 days time interval (and highlight the dynamics which takes place during day 1 by means of 4 different time points at 6, 12, 18, and 24h). Finally, we have assumed micro-scale periodicity, which is a limitation of the present model. It allows us to deal with complicated and potentially tortuous microvessels that are often encountered when dealing with vascularised cancer, as shown by Penta *et al.* (2015); Jain *et al.* (2007).

This paper is structured into different sections that are organized as follows. In Section 2 we describe the mathematical model by emphasizing the main assumptions and underlying physical phenomena. These include the differential equations for fluid flow, particle transport and heat convection in both the tumour vessels and the interstitial compartment. We also address the fluid, drug, and heat exchange taking place across the interface via setting up appropriate interface conditions. In Section 3, the differential equations are formulated in non-dimensional form. In Section 4, we apply the asymptotic homogenisation technique and derive the macro-scale results, which are then summarized in Section 5. In Section 6, we briefly discuss how the homogenised coefficients are determined on the basis of a microstructure. In Section 7, the differential equations describing particle and heat transport are written in spherical coordinates and supplemented by corresponding macro-scale initial and boundary conditions. In Section 8, the results obtained via numerical simulations are illustrated and discussed. In Section 9, concluding remarks are presented.

2. Mathematical modeling

In this work, we address mathematical modelling of cancer hyperthermia therapy carried out via nanoparticles delivery. We represent the vascularised tumor as a three-dimensional domain $\Omega \subseteq \mathbb{R}^3$. The tumour tissue comprises two regions. The interstitium is denoted here by Ω_t and the blood vessels' network by Ω_v, such that $\bar{\Omega}_t \cap \bar{\Omega}_v = \bar{\Omega}$.

The tumour system under consideration is multi-scale in nature and the typical distance between adjacent blood vessels $d \approx (50 - 100)\,\mu m$ is much smaller than the average size $L \approx 0.5\,cm$ of the cancerous region, as reported by Penta & Ambrosi (2015). Therefore, we define the small parameter

$$\varepsilon = \frac{d}{L} \ll 1. \tag{2.1}$$

We are interested in describing heat transport and the subsequent temperature distribution, which is driven by nanoparticles that are considered as being transported as passive scalars. Therefore, we can assume that delivery of nanoparticles is occurring via diffusion through both the vessels and the interstitium, advection due to the fluid flow in both compartments and extravasation across the vessels' walls. In the next section, we illustrate the governing equations for fluid, drug and heat transport in both the vessels and the interstitial space.

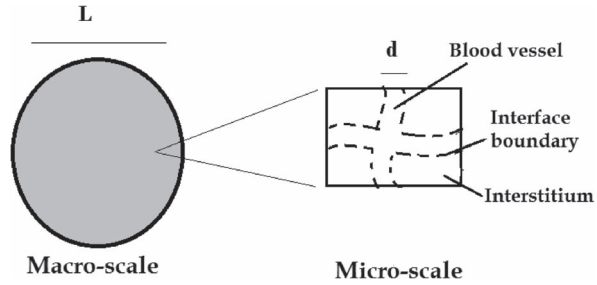

FIG. 1. A schematic comparing the domain at the micro-scale (comprising the interstitial space and the vessels) on the right, and the macro-scale domain, where the difference between the tumour constituents are homogenised, on the left.

All the variables in this model such as the pressure P, the concentration c, the velocity $\mathbf{u}$ and the temperature T are functions of both $\mathbf{x}$ and t.

2.1 *Interstitial fluid transport*

The tumour interstitial region is represented as an isotropic porous medium governed by Darcy's law:

$$\mathbf{u}_t = -\kappa \nabla P_t \quad in \quad \Omega_t, \tag{2.2}$$

together with the incompressibility constraint

$$\nabla \cdot \mathbf{u}_t = 0 \quad in \quad \Omega_t, \tag{2.3}$$

where $\mathbf{u}_t$, κ and P_t are the interstitial fluid velocity, conductivity and pressure, respectively.

2.2 *Microvascular flow*

The blood flowing in small capillaries is considered an incompressible viscous fluid and it is transported in the body through the vessels. Although non-Newtonian effects may become relevant in small capillaries, we assume that the blood is a Newtonian fluid as a first approximation, as done e.g. by Shipley & Chapman (2010). Therefore, the blood flow in the vessels can be described by the Stokes' problem, which, in absence of body forces, reads

$$\mu \nabla^2 \mathbf{u}_v = \nabla P_v \quad in \quad \Omega_v \tag{2.4}$$

$$\nabla \cdot \mathbf{u}_v = 0 \quad in \quad \Omega_v, \tag{2.5}$$

where $\mathbf{u}_v$, μ and P_v are the fluid velocity, viscosity and pressure in the blood vessels, respectively.

2.3 *Transport of particles*

The concentration dynamics of the particles in the vessels c_v can be described by the advection–diffusion equation in Ω_v. Absorption of particles in the interstitial compartment is represented by a linear uptake term. Therefore, the governing equations for the interstitial and vessels concentrations c_t

and c_v, respectively, read

$$\frac{\partial c_v}{\partial t} + \nabla \cdot (c_v \mathbf{u}_v - D_v \nabla c_v) = 0 \quad in \quad \Omega_v \tag{2.6}$$

$$\frac{\partial c_t}{\partial t} + \nabla \cdot (c_t \mathbf{u}_t - D_t \nabla c_t) = -\Lambda c_t \quad in \quad \Omega_t, \tag{2.7}$$

where D_v, D_t, and Λ are the particles' diffusivities in the vessels and in the interstitium and the uptake rate, respectively.

2.4 *Heat convection in the tumour*

The heat generated in the tumour is driven by application of a magnetic field that affects the nanoparticles injected into the bloodstream. When the magnetic field is removed, the magnetization of the particles returns to zero. The relaxation can take place either via the particle's rotation around the fluid (Brownian relaxation), or rotation of the magnetic moment around each particle (Neel relaxation), as explained e.g. by Pankhurst *et al.* (2003). These rotations generate the heat that provides an increase in temperature.

The temperatures in the vessel T_v and in the interstitium T_t are determined by a system of advection–diffusion equations. The heat generated by the magnetic field is represented by the heat source $\alpha f(c_{t,v})$ and, for the sake of simplicity, here we assume

$$f(c_{t,v}) = c_{t,v}. \tag{2.8}$$

The efficacy of the heat produced by the IONP depends on the absorption rate α (Nabil & Zunino, 2016). The latter parameter is in turn related to magnetic field properties (such as intensity and frequency) and particles' shape, although such features are not explicitly taken into account in the present work. The coupled system of PDEs then reads

$$\frac{\partial T_t}{\partial t} + \nabla \cdot \left(T_t \mathbf{u}_t - \frac{K_t}{\gamma_t \rho_t} \nabla T_t\right) = \frac{\alpha}{\gamma_t \rho_t} c_t \quad in \quad \Omega_t \tag{2.9}$$

$$\frac{\partial T_v}{\partial t} + \nabla \cdot \left(T_v \mathbf{u}_v - \frac{K_v}{\gamma_v \rho_v} \nabla T_v\right) = \frac{\alpha}{\gamma_v \rho_v} c_v \quad in \quad \Omega_v. \tag{2.10}$$

Here, K_t and K_v are the thermal conductivities in the interstitium and in the vessels, respectively. The parameters ρ_t and γ_t are the tissue density and specific heat capacity, while ρ_v, γ_v are the blood density and the blood specific heat capacity.

2.5 *Interface conditions*

The interface between the two domains is denoted by $\Gamma = \partial\Omega_v \cap \partial\Omega_t$. The fluid flow across the vessel is assumed to be continuous and depending on the pressures' difference between the two domains. We assume that the blood flux across the vessel wall is determined by Starling's law, i.e.

$$\mathbf{u}_t \cdot \mathbf{n} = \mathbf{u}_v \cdot \mathbf{n} = L_p(P_v - P_t) \quad on \quad \Gamma. \tag{2.11}$$

The vector $\mathbf{n}$ represents the unit outward vector normal to the vessels' wall. The parameter L_p represents the permeability of the blood vessels, which reflects the leakage of the vessels' wall. In order to close the problem we need to specify a condition for the tangent component of the fluid velocity to account for slip over the porous interface. We assume a Beavers and Joseph condition as done by Shipley & Chapman (2010); Penta *et al.* (2015), i.e.

$$\mathbf{u}_v \cdot \tau = -\frac{\sqrt{k}}{\varphi}\left[(\mathbf{n}\cdot\nabla)\mathbf{u}_v\right]\cdot\tau \quad on \quad \Gamma, \tag{2.12}$$

where φ is a non-dimensional parameter and τ denotes both of the unit vectors tangent to the vessels' walls. The parameter k is the tissue permeability, which is related to the hydraulic conductivity κ by the following relationship

$$\kappa = \frac{k}{\mu}. \tag{2.13}$$

The particles' flux is assumed to be continuous and proportional to the particles' concentration difference between the vessels and tumour:

$$(c_v\mathbf{u}_v - D_v\nabla c_v)\cdot\mathbf{n} = (c_t\mathbf{u}_t - D_t\nabla c_t)\cdot\mathbf{n} = p(c_v - c_t) \quad on \quad \Gamma, \tag{2.14}$$

where p is the diffusive membrane permeability. In this work, transvascular advection across the vessels' membrane, as investigated for instance by Mascheroni & Penta (2017), is neglected for the sake of simplicity, although the theoretical derivation that follows could be readily extended to such contributions.

The heat flux is likewise expressed in terms of the temperature difference between the two domains Ω_t and Ω_v as follows

$$\left(T_v\mathbf{u}_v - \frac{K_v}{\gamma_v\rho_v}\nabla T_v\right)\cdot\mathbf{n} = \frac{\beta}{\gamma_v\rho_v}\left(T_v - T_t\right) \quad on \quad \Gamma, \tag{2.15}$$

$$\left(T_t\mathbf{u}_t - \frac{K_t}{\gamma_t\rho_t}\nabla T_t\right)\cdot\mathbf{n} = \frac{\beta}{\gamma_t\rho_t}\left(T_v - T_t\right) \quad on \quad \Gamma, \tag{2.16}$$

where β is the heat transfer coefficient.

3. Non-dimensional form of the model

In this section we perform a non-dimensional analysis of the system of PDEs (2.2)–(2.10) supplemented with interface conditions (2.11)–(2.12) and (2.14–2.16) as follows:

$$\mathbf{u}_z = \frac{Cd^2}{\mu}\mathbf{u}_z', \quad P_z = CLP_z', \quad \nabla = \frac{1}{L}\nabla', \quad t = \frac{L\mu}{Cd^2}t', \quad c_z = C_r c_z', \quad T_z = TT_z'. \tag{3.1}$$

The index $z = v, t$ denotes either the vessels or the tumour, while C_r, T, C, d and L are the reference concentration, temperature, pressure gradient, inter-capillary distance and average tumour size, respectively.

By dropping the primes for the sake of simplicity of notation, the dimensionless PDEs can be written as:

$$\varepsilon^2\nabla^2\mathbf{u}_v = \nabla P_v \quad in \quad \Omega_v \tag{3.2}$$

$$\nabla\cdot\mathbf{u}_v = 0 \quad in \quad \Omega_v \tag{3.3}$$

$$\mathbf{u}_t = -\bar{\kappa}\nabla P_t \quad in \quad \Omega_t \tag{3.4}$$

$$\nabla\cdot\mathbf{u}_t = 0 \quad in \quad \Omega_t \tag{3.5}$$

$$\frac{\partial c_v}{\partial t} + \nabla\cdot(c_v\mathbf{u}_v - \bar{D}_v\nabla c_v) = 0 \quad in \quad \Omega_v \tag{3.6}$$

$$\frac{\partial c_t}{\partial t} + \nabla\cdot(c_t\mathbf{u}_t - \bar{D}_t\nabla c_t) = -\Upsilon c_t \quad in \quad \Omega_t \tag{3.7}$$

$$\frac{\partial T_v}{\partial t} + \nabla\cdot\left(T_v\mathbf{u}_v - \bar{K}_v\nabla T_v\right) = \bar{\alpha}_v c_v \quad in \quad \Omega_v \tag{3.8}$$

$$\frac{\partial T_t}{\partial t} + \nabla\cdot\left(T_t\mathbf{u}_t - \bar{K}_t\nabla T_t\right) = \bar{\alpha}_t c_t \quad in \quad \Omega_t, \tag{3.9}$$

with boundary conditions:

$$\mathbf{u}_v\cdot\tau = -\varepsilon\bar{\varphi}[(\mathbf{n}\cdot\nabla)\mathbf{u}_v]\cdot\tau \quad on \quad \Gamma \tag{3.10}$$

$$\mathbf{u}_v\cdot\mathbf{n} = \varepsilon\bar{L}(P_v - P_t) \quad on \quad \Gamma \tag{3.11}$$

$$\mathbf{u}_t\cdot\mathbf{n} = \varepsilon\bar{L}(P_v - P_t) \quad on \quad \Gamma \tag{3.12}$$

$$(c_v\mathbf{u}_v - \bar{D}_v\nabla c_v)\cdot\mathbf{n} = \varepsilon\bar{p}(c_v - c_t) \quad on \quad \Gamma \tag{3.13}$$

$$(c_t\mathbf{u}_t - \bar{D}_t\nabla c_t)\cdot\mathbf{n} = \varepsilon\bar{p}(c_v - c_t) \quad on \quad \Gamma \tag{3.14}$$

$$\left(T_v\mathbf{u}_v - \bar{K}_v\nabla T_v\right)\cdot\mathbf{n} = \varepsilon\bar{\beta}_v\left(T_v - T_t\right) \quad on \quad \Gamma \tag{3.15}$$

$$\left(T_t\mathbf{u}_t - \bar{K}_t\nabla T_t\right)\cdot\mathbf{n} = \varepsilon\bar{\beta}_t\left(T_v - T_t\right) \quad on \quad \Gamma, \tag{3.16}$$

where the primes have been dropped for the sake of simplicity.

The non-dimensional numbers are defined as:

$$\bar{L} = \frac{L_p L^2\mu}{d^3}, \quad \bar{\kappa} = \frac{\kappa\mu}{d^2}, \quad \bar{\varphi} = \frac{\sqrt{\bar{\kappa}}}{\varphi}, \bar{p} = \frac{pL\mu}{Cd^3}, \quad \Upsilon = \frac{\Lambda\mu}{LCd^2}, \tag{3.17}$$

$$\bar{\alpha}_v = \frac{\alpha C_r L\mu}{\rho_v\gamma_v TCd^2}, \quad \bar{\alpha}_t = \frac{\alpha C_r L\mu}{\rho_t\gamma_t TCd^2}, \quad \bar{\beta}_v = \frac{\beta L\mu}{\rho_v\gamma_v Cd^3}, \quad \bar{\beta}_t = \frac{\beta L\mu}{\rho_t\gamma_t Cd^3}. \tag{3.18}$$

Here, $\bar{\kappa}$ is the non-dimensional hydraulic conductivity. The coefficients Υ and $\bar{\alpha}$ are non-dimensional uptake rate and absorption rate. The numbers $\bar{L}$, $\bar{p}$, $\bar{\beta}$ and $\bar{\varphi}$ are the non-dimensional vessels' hydraulic

and diffusive permeabilities, heat transfer and Beavers and Joseph coefficients, respectively. The non-dimensional diffusivities of the particles in the vessels and the tumour are the reciprocal of their corresponding Peclet's numbers, i.e.

$$\bar{D}_{v,t} = \frac{1}{Pe_{v,t}}, \tag{3.19}$$

where

$$Pe_v = \frac{LCd^2}{D_v\mu}, \qquad Pe_t = \frac{LCd^2}{D_t\mu}. \tag{3.20}$$

The non-dimensional thermal conductivities are given by

$$\bar{K}_{v,t} = \frac{K_{v,t}\mu}{\rho_{v,t}\gamma_{v,t}LCd^2}. \tag{3.21}$$

The ε scaling appearing on the right hand side of interface conditions equations (3.11–3.16) is the appropriate one to ensure that blood, drug and heat fluxes inside the tumour stays finite in the limit $\varepsilon \to 0$, as observed by Penta *et al.* (2015). Furthermore, we assume that the parameters appearing in equations (3.17–3.21) are finite in the limit as ε approaches zero. This is done consistently with the approach carried out by Penta *et al.* (2015) and ensures that both drug and thermal diffusivities, which are well known to play a crucial role in the nanoparticles' dynamics, are captured at leading order. There exist different scaling choices in the literature, see, e.g. the work by Shipley & Chapman (2010), where the authors perform the upscaling of the equations describing fluid and drug transport in vascularised tumours and their choice concerning distinguished limits of the Peclet's numbers results in a suite of reaction–advection models.

4. The asymptotic homogenisation method

The asymptotic homogenisation method is an upscaling strategy that provides a macro-scale description of a given physical system informed by the microstructure. It has been successfully applied to a large variety of real-world scenarios including previous investigations related to fluid and drug transport in biological tissues and vascularised tumours, as done, e.g. by Shipley & Chapman (2010); Penta *et al.* (2014, 2015); Penta & Ambrosi (2015); O'Dea *et al.* (2015); Mascheroni & Penta (2017); Penta & Merodio (2017); Dalwadi & King (2020).

In our model, the application of the multi-scale method is motivated by large difference in sizes between the inter-vessels distance and the tumour radius, as assumed by Shipley & Chapman (2010); Penta *et al.* (2015). In particular, we assume that these two scales are well separated, so that the small parameter ε defined in equation (2.1) is much smaller than 1. Therefore, we can define two formally independent variables $\mathbf{y}$ (the micro-scale) and $\mathbf{x}$ (the macro-scale) related by:

$$\mathbf{y} = \frac{\mathbf{x}}{\varepsilon}.$$

Following the above-mentioned previous works, we enforce periodicity with respect to the micro-scale variable $\mathbf{y}$, and we assume that every unknown field can be represented in power series of ε as:

$$\upsilon(\mathbf{x},t) \equiv \upsilon^{(\varepsilon)}(\mathbf{x},\mathbf{y},t) = \sum_{l=0}^{\infty} \upsilon^{(l)}(\mathbf{x},\mathbf{y},t)\varepsilon^l = \upsilon^{(0)}(\mathbf{x},\mathbf{y},t) + \varepsilon\upsilon^{(1)}(\mathbf{x},\mathbf{y},t) + \varepsilon^2\upsilon^{(2)}(\mathbf{x},\mathbf{y},t) + \ldots \quad , \tag{4.1}$$

where υ collectively represents any variable described in our model namely P_z, c_z, $\mathbf{u}_z$ or T_z, (with $z = v, t$).

The differential operators transform according to the chain rule:

$$\nabla \to \nabla_x + \frac{1}{\varepsilon}\nabla_y; \qquad \nabla^2 \to \frac{1}{\varepsilon^2}\nabla_y + \frac{2}{\varepsilon}\nabla_y \cdot \nabla_x + \nabla_x^2. \tag{4.2}$$

We equate the same power of ε^l, $(l = 0, 1, 2, \ldots)$ to find suitable differential equations in order to close the problem for the leading order variables $P_v^{(0)}$, $P_t^{(0)}$, $\mathbf{u}_v^{(0)}$, $\mathbf{u}_t^{(0)}$, $c_v^{(0)}$, $c_t^{(0)}$, $T_v^{(0)}$ and T_t^0. As we would like to obtain a system defined on the macro-scale only, for fields that retain a dependence on the micro-scale variable $\mathbf{y}$, we can integrate over the periodic cell. From now on, since we are assuming micro-scale periodicity, Ω_v and Ω_t represent the vessels and interstitium cell portions, respectively, and the micro-scale cell average is defined by:

$$\langle \upsilon \rangle_z = \frac{1}{|\Omega_z|}\int_{\Omega_z} \upsilon(\mathbf{x},\mathbf{y},t)\,\mathrm{d}y, \quad z = t, v, \tag{4.3}$$

where $|\Omega_v|$ and $|\Omega_t|$ are the vessels and interstitial cell volumes' portions. In particular, we assume that all the fields $\upsilon^{(l)}$, $l = 0, 1, \ldots$ are $\mathbf{y}$-periodic.

The cell volume fraction $|\Omega_v|(\mathbf{x})$, $|\Omega_t|(\mathbf{x})$, and the surface area of the interface $S(\mathbf{x})$ are defined by,

$$S(\mathbf{x}) = \int_{\Gamma} \mathrm{d}S_y,$$

$$|\Omega_{v,t}|(\mathbf{x}) = \int_{\Omega_{v,t}} \mathrm{d}V_y.$$

In our case we enforce macroscopic uniformity such that S, $|\Omega_t|$,$|\Omega_v|$ are constant. Analyses of non-macroscopically uniform structures are beyond the scope of this work; however, they could be relevant in several contexts and alternative approaches to deal with such heterogeneities can be found in the works by Penta *et al.* (2014, 2015); Dalwadi & King (2020), and the references therein.

5. The macro-scale model obtained via asymptotic homogenisation

By applying the asymptotic homogenisation steps described in the previous section to the system of equations 3.23.9 with boundary condition (3.11)–(3.16) we obtain the macro-scale differential equations

for the zero-th order pressures, velocities, concentrations and temperatures $P_t^{(0)}$, $P_v^{(0)}$, $\langle \mathbf{u}_t^{(0)} \rangle_t$, $\langle \mathbf{u}_v^{(0)} \rangle_v$, $c_t^{(0)}$, $c_v^{(0)}$, $T_t^{(0)}$ and $T_v^{(0)}$. These can be summarized as follows, while for the full derivation of the model, which is carried out by generalizing the methodology carried by Penta *et al.* (2015) to heat transport equations with a concentration-dependent source, the reader can refer to Appendices A and B.

$$\begin{cases} \langle \mathbf{u}_v^{(0)} \rangle_v = -\mathsf{Y}_v \nabla_x P_v^{(0)} \\ \langle \mathbf{u}_t^{(0)} \rangle_t = -\bar{\kappa} \mathsf{Y}_t \nabla_x P_t^{(0)} \end{cases} \tag{5.1}$$

$$\begin{cases} \nabla_x \cdot \left(\mathsf{Y}_v \nabla_x P_v^{(0)} \right) = \frac{\bar{L}\left(P_v^{(0)} - P_t^{(0)}\right)}{|\Omega_v|} S \\ \nabla_x \cdot \left(\bar{\kappa} \mathsf{Y}_t \nabla_x P_t^{(0)} \right) = \frac{\bar{L}\left(P_t^{(0)} - P_v^{(0)}\right)}{|\Omega_t|} S \end{cases} \tag{5.2}$$

$$\begin{cases} \frac{\partial c_v^{(0)}}{\partial t} + \nabla_x \cdot \left(c_v^{(0)} \langle \mathbf{u}_v^{(0)} \rangle_v - \mathsf{F}_v \nabla_x c_v^{(0)} \right) + \frac{S}{|\Omega_v|} \bar{p} \left(c_v^{(0)} - c_t^{(0)} \right) = 0 \\ \frac{\partial c_t^{(0)}}{\partial t} + \nabla_x \cdot \left(c_t^{(0)} \langle \mathbf{u}_t^{(0)} \rangle_t - \mathsf{F}_t \nabla_x c_t^{(0)} \right) + \frac{S}{|\Omega_t|} \bar{p} \left(c_t^{(0)} - c_v^{(0)} \right) = -\Upsilon c_t^{(0)} \end{cases} \tag{5.3}$$

$$\begin{cases} \frac{\partial T_v^{(0)}}{\partial t} + \nabla_x \cdot \left(T_v^{(0)} \langle \mathbf{u}_v^{(0)} \rangle_v - \mathsf{N}_v \nabla_x T_v^{(0)} \right) + \frac{S}{|\Omega_v|} \bar{\beta}_v \left(T_v^{(0)} - T_t^{(0)} \right) = \bar{\alpha}_v c_v^{(0)} \\ \frac{\partial T_t^{(0)}}{\partial t} + \nabla_x \cdot \left(T_t^{(0)} \langle \mathbf{u}_t^{(0)} \rangle_t - \mathsf{N}_t \nabla_x T_t^{(0)} \right) + \frac{S}{|\Omega_t|} \bar{\beta}_t \left(T_t^{(0)} - T_v^{(0)} \right) = \bar{\alpha}_t c_t^{(0)}, \end{cases} \tag{5.4}$$

where $\mathsf{Y}_v(\mathbf{x})$, $\bar{\kappa}\mathsf{Y}_t(\mathbf{x})$, $\mathsf{F}_v(\mathbf{x})$, $\mathsf{F}_t(\mathbf{x})$, $\mathsf{N}_v(\mathbf{x})$, $\mathsf{N}_t(\mathbf{x})$ are effective hydraulic, diffusion and thermal conductivity tensors in the vessels' and interstitial compartments, respectively. Here, $|\Omega_v|$ denotes the vessel volume, $|\Omega_t|$ is the interstitial volume and S is the vessels' wall surface.

The system of equations (5.2) describes transport in a porous medium with mass transfer between compartments. The leakage of the blood across the vessels is reflected in the mass exchange between the two compartments, which is proportional to the difference between the leading order pressures.

The particles' transport in the vessels' and interstitial compartments depends on the fluid flow and it is represented by the system of coupled advection–diffusion–reaction equations (5.3).

Similarly, the system of coupled advection–diffusion–reaction equations in (5.4) describes the heat transport at the macro-scale and the temperatures' profiles depend on both fluid and particles' transport.

Moreover, the macro-scale coefficients, namely hydraulic conductivity tensors, diffusion tensors and thermal conductivity tensors, can be determined by solving the cell problems.

The hydraulic conductivities Y_v and the auxiliary tensor Y_t are defined as

$$\mathsf{Y}_v = \langle \mathsf{W} \rangle_v = \frac{1}{|\Omega_v|} \int_{\Omega_v} W \mathrm{d}y, \tag{5.5}$$

$$\mathsf{Y}_t = I - \frac{1}{|\Omega_t|} \int_{\Omega_t} (\nabla_y \mathbf{r})^T \mathrm{d}y \tag{5.6}$$

where the tensor W and vector $\mathbf{r}$ are satisfied the cell problems:

$$\nabla_y^2 \mathsf{W}^T = \nabla_y \mathbf{m} - I \quad in \quad \Omega_v \tag{5.7}$$

$$\nabla_y \cdot \mathsf{W}^T = 0 \quad in \quad \Omega_v \tag{5.8}$$

$$\mathsf{W}^T \cdot \mathbf{n} = 0 \quad on \quad \Gamma \tag{5.9}$$

$$\mathsf{W}^T \tau = -\bar{\varphi}[(\nabla_y \mathsf{W}^T)\mathbf{n}]\tau \quad on \quad \Gamma, \tag{5.10}$$

and,

$$\nabla_y^2 \mathbf{r} = 0 \quad in \quad \Omega_t \tag{5.11}$$

$$(\nabla_y \mathbf{r}) \cdot \mathbf{n}_t = \mathbf{n}_t \quad on \quad \Gamma, \tag{5.12}$$

where

$$\langle \mathbf{m} \rangle_v = 0 \quad in \quad \Omega_v, \quad \langle \mathbf{r} \rangle_t = 0 \quad in \quad \Omega_t. \tag{5.13}$$

The diffusivity tensors F_v and F_t are given by:

$$\mathsf{F}_v = \bar{D}_v (I - \langle (\nabla_y \mathbf{a})^T \rangle_v) \tag{5.14}$$

and

$$\mathsf{F}_t = \bar{D}_t (I - \langle (\nabla_y \mathbf{b})^T \rangle_t), \tag{5.15}$$

while the auxiliary variables $\mathbf{a}$ and $\mathbf{b}$ satisfy the cell problems:

$$\nabla_y^2 \mathbf{a} = 0 \quad in \quad \Omega_v \tag{5.16}$$

$$(\nabla_y \mathbf{a})\mathbf{n} = \mathbf{n} \quad on \quad \Gamma \tag{5.17}$$

$$\nabla_y^2 \mathbf{b} = 0 \quad in \quad \Omega_t \tag{5.18}$$

$$(\nabla_y \mathbf{b})\mathbf{n} = \mathbf{n} \quad on \quad \Gamma. \tag{5.19}$$

The thermal conductivities N_v, and N_t are defined as:

$$\mathsf{N}_v = \bar{K}_v (I - \langle (\nabla_y \mathbf{g})^T \rangle_v) \tag{5.20}$$

$$\mathsf{N}_t = \bar{K}_t (I - \langle (\nabla_y \mathbf{e})^T \rangle_t), \tag{5.21}$$

with

$$\nabla_y^2 \mathbf{g} = 0 \quad in \quad \Omega_v \tag{5.22}$$

$$(\nabla_y \mathbf{g})\mathbf{n} = \mathbf{n} \quad on \quad \Gamma \tag{5.23}$$

$$\nabla_y^2 \mathbf{e} = 0 \quad in \quad \Omega_t \tag{5.24}$$

$$(\nabla_y \mathbf{e})\mathbf{n} = \mathbf{n} \quad on \quad \Gamma. \tag{5.25}$$

For instance, the cell problems related to interstitial fluid flow, drug transport and heat transport are to be closed by a further condition for uniqueness to be achieved (e.g. by assuming the null cell average of the auxiliary variables in the cell), as illustrated by Cioranescu & Donato (1999); Penta *et al.* (2015).

6. The effective coefficients and micro-scale cell problems

In order to close the system of PDEs at the macro-scale, we need to compute the effective coefficients by solving appropriate cell problems at the micro-scale. The differential problems that are related to the hydraulic conductivity tensors are discussed by Penta & Ambrosi (2015). The authors solved the differential problems numerically and investigated the influence of the vessels' tortuosity on the hydraulic conductivity tensors. Mascheroni & Penta (2017) extended the analysis carried out by Penta & Ambrosi (2015) to compute the effective diffusion coefficients by solving the cell problems related to drug transport, i.e. finding the solution for the auxiliary variables that are called **a**, and **b** in the present manuscript, cf. (5.16)–(5.17), and (5.18)–(5.19). They also varied the geometrical tortuosity and found its impact on the tensors F_v and F_t. Changing the vessels' shape or tortuosity implies changes in the interstitial and vessels' volumes. Both the vessels' hydraulic conductivity and particles' diffusivity are affected by the vessels' tortuosity. In particular, Penta & Ambrosi (2015) show that the hydraulic conductivity exhibits a nonlinear decreasing profile at increasing tortuosity, while Mascheroni & Penta (2017) show that also diffusion decreases as tortuosity increases, although to a lesser extent. In contrast, the interstitial coefficients are not significantly affected by micro-scale changes in the geometry under consideration. Penta & Ambrosi (2015) solved the problem that corresponds to those related to the interstitial fluid, drug and thermal auxiliary variables **r**, **b** and **e** in our work, i.e. (5.12), (5.18)–(5.19) and (5.24)–(5.25), respectively. In particular, these latter problems (5.11)–(5.12), (5.18)–(5.19) and (5.24)–(5.25) are equivalent, so the auxiliary variables **r**, **b** and **e** solve the same problem and

$$\nabla_{\mathbf{y}} \mathbf{r} = \nabla_{\mathbf{y}} \mathbf{b} = \nabla_{\mathbf{y}} \mathbf{e}. \tag{6.1}$$

Penta & Ambrosi (2015) concluded that as long as the vessels' volume fraction is much smaller than the interstitial one, the influence of the micro-scale on the interstitial coefficients is negligible, i.e. they observed that

$$\langle \nabla_{\mathbf{y}} \mathbf{r} \rangle_t = \langle \nabla_{\mathbf{y}} \mathbf{b} \rangle_t = \langle \nabla_{\mathbf{y}} \mathbf{e} \rangle_t \approx 0. \tag{6.2}$$

As such, from now on we focus on the micro-scale cell problems in the vessels' compartments and account for (6.2), so that, by recalling the definitions (5.6), (5.15) and (5.21), we can assume

$$\mathsf{Y}_t = \mathsf{I}; \quad \mathsf{F}_t = \bar{D}_t \mathsf{I}; \quad \mathsf{N}_t = \bar{K}_t \mathsf{I}. \tag{6.3}$$

By following Penta & Ambrosi (2015); Mascheroni & Penta (2017), we enforce invariance with respect to the three orthogonal axes so that the auxiliary tensors in the vessels $\mathsf{W}, \mathsf{F}_v, \mathsf{N}_v$ are proportional to the identity tensor.

In particular, for the diffusivity F_v and thermal conductivity N_v, we have:

$$\mathsf{F}_v = \tilde{D}_v \mathsf{I}, \quad \mathsf{N}_v = \tilde{N}_v I,$$

such that:

$$\tilde{D}_v = \bar{D}_v \left(1 - \langle \frac{\partial a_1}{\partial y_1} \rangle_v\right) = \bar{D}_v \left(1 - \langle \frac{\partial a_2}{\partial y_2} \rangle_v\right) = \bar{D}_v \left(1 - \langle \frac{\partial a_3}{\partial y_3} \rangle_v\right),$$

$$\tilde{N}_v = \bar{K}_v \left(1 - \langle \frac{\partial g_1}{\partial y_1} \rangle_v\right) = \bar{K}_v \left(1 - \langle \frac{\partial g_2}{\partial y_2} \rangle_v\right) = \bar{K}_v \left(1 - \langle \frac{\partial g_3}{\partial y_3} \rangle_v\right),$$

where we can further notice that **a** and **g** are actually the solution to the exact same cell problem (5.16–5.17) or equivalently (5.22–5.23). This leads to the solution of a standard Laplace problem, which reads, e.g. for the component g_1:

$$\nabla^2 g_1 = 0 \quad in \quad \Omega_v \tag{6.4}$$

$$\nabla g_1 \cdot \mathbf{n} = n_1 \quad on \quad \Gamma \tag{6.5}$$

supplemented by a further condition to ensure uniqueness, e.g.

$$\langle g_1 \rangle_v = 0 \quad in \quad \Omega_v.$$

The analysis that follows is carried out by varying the tortuosity of the microvessels according to Penta & Ambrosi (2015). In particular, the center line of every vessel is defined as:

$$f(s) = A \sin(2\pi \omega s / l),$$

where A is the amplitude, ω is the frequency, s is the local parametrization along the branch and l is branch length and we have $0 \leq s \leq l$. The tumour interstitium is the domain that is complementary to vessels' compartment in the cubic cell.

We exploit the solutions of the cell problem 6.4–6.5, which is solved by Mascheroni & Penta (2017), to investigate the role of tortuosity on the homogenised thermal conductivity $\tilde{N}_v$ by varying the amplitude and spatial frequency ω. The profile of the relative thermal conductivity (and diffusivity)

$$\tilde{D}_v / \bar{D}_v = \tilde{N}_v / \bar{K}_v = 1 - \langle \frac{\partial a_1}{\partial y_1} \rangle_v = 1 - \langle \frac{\partial g_1}{\partial y_1} \rangle_v, \tag{6.6}$$

which is based on the results reported by Mascheroni & Penta (2017), is shown in Fig. 2.

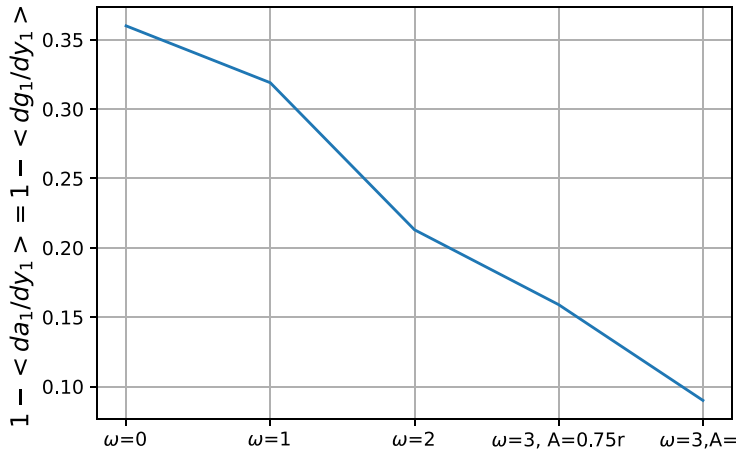

FIG. 2. Ratio between the homogenised and base vessels' diffusive conductivities values.

7. The mathematical model for a spherical tumour

We assume that the vascularised tumour can be represented in spherical coordinates with radius R. Also, we presume that the symmetric tumour is isolated and it interacts with surrounding environment through the vessels. Assuming radial symmetry, the model reads as follows:

$$\begin{cases} \frac{\partial c_v^{(0)}}{\partial t} + \frac{1}{r^2}\frac{\partial}{\partial r}\left(r^2\left(c_v^{(0)}\langle u_v^{(0)}\rangle_v - \tilde{D}_v\frac{\partial c_v^{(0)}}{\partial r}\right)\right) + \frac{S}{|\Omega_v|}\bar{p}\left(c_v^{(0)} - c_t^{(0)}\right) = 0 \quad in \quad \Omega_v \\ \frac{\partial T_v^{(0)}}{\partial t} + \frac{1}{r^2}\frac{\partial}{\partial r}\left(r^2\left(T_v^{(0)}\langle u_v^{(0)}\rangle_v - \tilde{N}_v\frac{\partial T_v^{(0)}}{\partial r}\right)\right) + \frac{S}{|\Omega_v|}\bar{\beta}_v\left(T_v^{(0)} - T_t^{(0)}\right) = \bar{\alpha}_v c_v^0 \quad in \quad \Omega_v \end{cases} \tag{7.1}$$

$$\begin{cases} \frac{\partial c_t^{(0)}}{\partial t} + \frac{1}{r^2}\frac{\partial}{\partial r}\left(r^2\left(c_t^{(0)}\langle u_t^{(0)}\rangle_t - \bar{D}_t\frac{\partial c_t^{(0)}}{\partial r}\right)\right) + \frac{S}{|\Omega_t|}\bar{p}\left(c_t^{(0)} - c_v^{(0)}\right) = -\Upsilon c_t^{(0)} \quad in \quad \Omega_t \\ \frac{\partial T_t^{(0)}}{\partial t} + \frac{1}{r^2}\frac{\partial}{\partial r}\left(r^2\left(T_t^{(0)}\langle u_t^{(0)}\rangle_t - \bar{K}_t\frac{\partial T_t^{(0)}}{\partial r}\right)\right) + \frac{S}{|\Omega_t|}\bar{\beta}_t\left(T_t^{(0)} - T_v^{(0)}\right) = \bar{\alpha}_t c_t^{(0)} \quad in \quad \Omega_t, \end{cases} \tag{7.2}$$

where $0 \leqslant r \leq R$ and $0 \leqslant t \leqslant \mathscr{T}$, where $\mathscr{T}$ is the time interval under investigation.

The macro-scale system describing the fluid transport (5.1–5.2) was solved analytically when accounting for spherical symmetry by Penta & Ambrosi (2015). In this case, the system to be solved reads (neglecting from now on the labelling indicating the leading order character of every field $^{(0)}$ for the sake of simplicity of notation):

$$\frac{1}{r}\frac{d^2}{dr^2}(rP_v) = M_v(P_v - P_t) \quad in \quad \Omega_v \tag{7.3}$$

$$\frac{1}{r}\frac{d^2}{dr^2}(rP_t) = -M_t(P_v - P_t) \quad in \quad \Omega_t \tag{7.4}$$

$$u_v(r) = -H_v \frac{dP_v}{dr} \quad in \quad \Omega_v \tag{7.5}$$

$$u_t(r) = -\tilde{H}_t \frac{dP_t}{dr} \quad in \quad \Omega_t \tag{7.6}$$

$$\frac{dP_v}{dr}|_{r=0} = \frac{dP_t}{dr}|_{r=0} = 0 \tag{7.7}$$

$$P_v|_{r=R} = \bar{P} > 0, \quad P_t|_{r=R} = 0. \tag{7.8}$$

The above system of equation was solved by Penta & Ambrosi (2015) by accounting for boundary conditions that are consistent with Jain *et al.* (2007) and the references therein, i.e. those for an isolated tumour with fluid flow driven by the difference between the vascular and the interstitial pressures (the vascular pressure is actually considered constant in Jain *et al.* (2007) and the references therein). In the above, H_v is the vessels' hydraulic conductivity parameter, which, according to Penta & Ambrosi (2015), ranges from $2.20 \cdot 10^{-4}$ for a regular microvasculature to $4.89 \cdot 10^{-6}$ for the most tortuous scenario, and satisfies:

$$\mathsf{Y}_v = H_v I, \quad H_v = \langle \mathsf{W}_{11} \rangle_v = \langle \mathsf{W}_{22} \rangle_v = \langle \mathsf{W}_{33} \rangle_v, \tag{7.9}$$

where $\mathsf{Y}_v = \langle \mathsf{W} \rangle_v$ as derived in Appendix A.

The parameter $\tilde{H}_t = \bar{\kappa} H_t$, where

$$\mathsf{Y}_t = H_t I, \quad H_t = \langle \mathsf{Y}_{t11} \rangle_v = \langle \mathsf{Y}_{t22} \rangle_v = \langle \mathsf{Y}_{t33} \rangle_v, \tag{7.10}$$

and $H_t = 1$ in our case by means of (6.2).

The solutions of the system (7.3)–(7.8) derived by Penta & Ambrosi (2015) are summarized below.

$$P_v = \frac{1}{M_v + M_t} \left(M_t + \frac{M_v \sinh(\tilde{\alpha}\hat{r})}{\hat{r} \sinh(\tilde{\alpha})} \right), \tag{7.11}$$

$$P_t = \frac{M_t}{M_v + M_t} \left(1 - \frac{\sinh(\tilde{\alpha}\hat{r})}{\hat{r} \sinh(\tilde{\alpha})} \right), \tag{7.12}$$

where $\hat{r} = r/R$ (Relative radius position), and

$$\tilde{\alpha} = R\sqrt{(M_v + M_t)}, \tag{7.13}$$

with

$$M_v = \frac{\bar{L}S}{H_v |\Omega_v|}, \quad M_t = \frac{\bar{L}S}{\tilde{H}_t |\Omega_t|}.$$

7.1 *Initial and boundary conditions*

We assume that no particle is present in the whole system at $t = 0$. Also, both the drug and the heat fluxes must vanish in the tumour centre as a consequence of the radial symmetry assumption. We assume a vessels' bolus injection with clearance time ς at the boundary of the macro-scale domain, which means that the concentration of the particles declines exponentially due to body elimination effects in the plasma, as shown by Chou *et al.* (2013). We also assume the continuity of particles' concentration at the boundary of the interstitial region. The initial temperatures are set to be the standard vessels' temperature $310.15K$. Following the approach by Nabil & Zunino (2016), we impose Robin condition on the boundary of the tumour interstitium to account for the heat transfer between the tumour and the vessels' mediated by intermediate layers of tissue (Nabil & Zunino, 2016; Cervadoro *et al.*, 2013; Saeedi *et al.*, 2017; Kaddi *et al.*, 2013). The initial and boundary conditions can be summarized as follows

$$\begin{cases} c_t|_{t=0} = c_v|_{t=0} = 0 \\ \left(u_v c_v - \tilde{D}_v \frac{\partial c_v}{\partial_r}\right)\Big|_{r=0} = \left(u_t c_t - \bar{D}_t \frac{\partial c_t}{\partial_r}\right)\Big|_{r=0} = 0 \\ c_v|_{r=R} = e^{-t/\varsigma}, \quad c_t|_{r=R} = c_v, \end{cases} \tag{7.14}$$

and,

$$\begin{cases} T_v|_{t=0} = T_t|_{t=0} = 1 \\ v\left(u_v T_v - \tilde{N}_v \frac{\partial T_v}{\partial r}\right)\Big|_{r=0} = \left(u_t T_t - \bar{K}_t \frac{\partial T_r}{\partial r}\right)\Big|_{r=0} = 0. \\ T_v|_{r=R} = 1, \qquad \left(u_t T_t - \bar{K}_t \frac{\partial T_r}{\partial t}\right)\Big|_{r=R} = \bar{\beta}_t (T_v - T_t). \end{cases} \tag{7.15}$$

The finite element software Comsol Multiphysics is used to solve the model and the values of the parameters are provided in Table 1.

We have used the finite element commercial software COMSOL Multiphysics, version 4.3a, and both the drug and the heat transport systems (7.1)–(7.2) have been implemented by means of the convection–diffusion module in coefficient form equipped with boundary and initial conditions (7.14)–(7.15) and parameters taken from Table 1. The spatial discretization is carried out by means of P2 elements, while for the discretization in time an implicit backward differentiation formula method is embraced, similarly to Mascheroni & Penta (2017). Although the system is solved in non-dimensional form, the temperatures and the absorption rate are shown in dimensional form in the plots to foster the Reader's clarity in terms of comparison against the previous literature.

8. Results and discussion

Mascheroni & Penta (2017) studied the macromolecules distribution in both the vessels and the interstitial compartment using the advection–diffusion–reaction equations derived by Penta *et al.* (2015). The reaction terms are related to the uptake of anti-cancer agents, as well as additional contributions due to the upscaling of transvascular diffusion of particles. The authors presented the result for a spherical tumour, and they discussed the impact of tortuosity on drug transport.

In the present work, we extend the works by Penta *et al.* (2015); Mascheroni & Penta (2017) to heat transport and solve the resulting systems of PDEs to obtain the temperature maps that are driven by nanoparticles' transport in the context of cancer hyperthermia. Although also the drug transport analysis carried out here differs from the one by Mascheroni & Penta (2017) in terms of the choice of

TABLE 1 *List of parameters and their values*

Symbols	Parameter	Value	Unite	Reference
μ	Blood viscosity	4×10^{-3}	$Pa \cdot s$	Nabil & Zunino (2016)
L_p	Vessels' permeability	1.78×10^{-11}	$m/(Pa \cdot s)$	Mascheroni & Penta (2017)
κ	Tumour hydraulic conductivity	2.1×10^{-13}	$m^2/(Pa \cdot s)$	Mascheroni & Penta (2017)
D_v	Diffusivity of the nanoparticles in the capillaries	3.3×10^{-10}	m^2/s	Mascheroni & Penta (2017)
D_t	Diffusivity of the nanoparticles in the interstitium	1.0×10^{-11}	m^2/s	Mascheroni & Penta (2017)
K_t	Thermal conductivity of the tumour	0.52	$W/(m \cdot K)$	Tang *et al.* (2018)
K_v	Thermal conductivity of the vessels	0.51	$W/(m \cdot K)$	Tang *et al.* (2018)
β	Heat transfer coefficient	20	$W/(m^2 \cdot K)$	Nabil & Zunino (2016)
Λ	Uptake rate in the tumour	1.07×10^{-11}	s^{-1}	Mascheroni & Penta (2017)
p	Diffusive permeability of the membrane	1.7×10^{-7}	m/s	Mascheroni & Penta (2017)
d	Reference micro-scale	4.0×10^{-5}	m	Mascheroni & Penta (2017)
L	Reference macro-scale	1.0×10^{-2}	m	Mascheroni & Penta (2017)
C	Reference pressure gradient	5×10^2	Pa/m	Mascheroni & Penta (2017)
ς	Reference plasma clearance time	432	s	Mascheroni & Penta (2017)
α	Absorption rate	6×10^6	W/Kg	Cervadoro *et al.* (2013)
γ_t	Tissue's specific heat	3470	$J/(Kg \cdot K)$	Nabil & Zunino (2016)
ρ_t	Tissue's density	1060	Kg/m^3	Nabil & Zunino (2016)
γ_v	Vessels' specific heat	3617	$J/(Kg \cdot K)$	Miaskowski & Sawicki (2013)
ρ_v	Vessels' density	1050	Kg/m^3	Miaskowski & Sawicki (2013)
C_r	Reference concentration	100	mg/ml	De la Presa *et al.* (2012)
T	Reference blood temperature	310.15	K	

parameters (which are related to nanoparticles and macromolecules, respectively), as well as macro-scale boundary conditions (we assume continuity of concentrations at the tumour boundary as done by Penta & Ambrosi (2015) here, while zero diffusive interstitial drug flux is assumed by Mascheroni & Penta (2017)), a qualitative comparison concerning the drug transport problem is still possible, and provides a benchmark supporting the reliability of the results presented here.

We commence by first presenting our results concerning the solution of the drug transport problem and then show the results concerning temperatures maps against the relative radial position at varying microvessels' tortuosity and absorption rate.

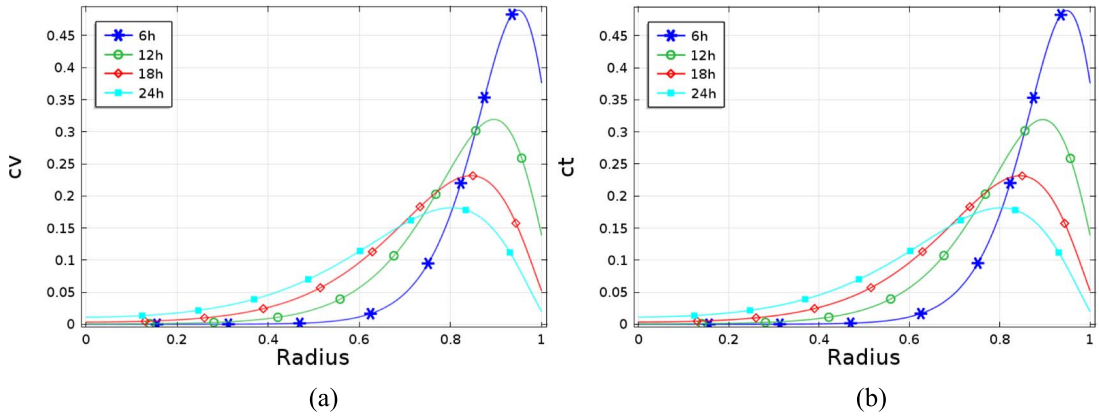

FIG. 3. Vessels (a) and interstitial (b) particles distribution vs tumour radius—low uptake rate case, and period of 24 h.

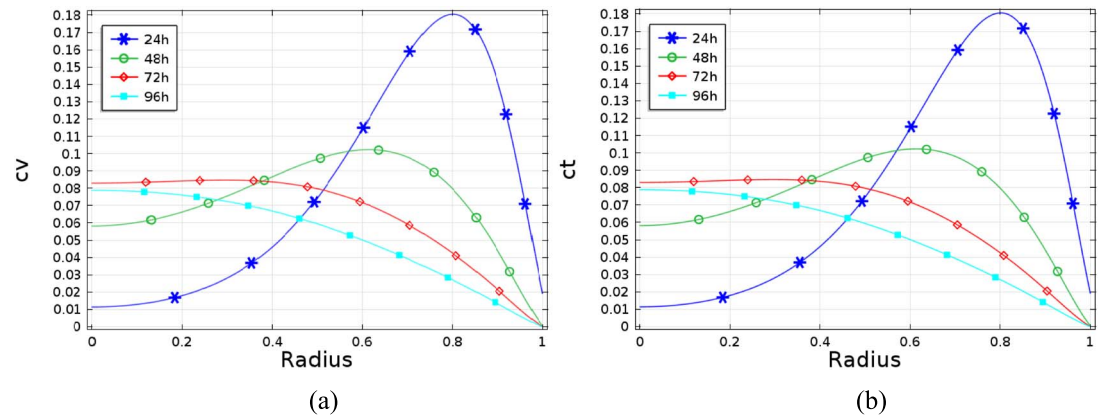

FIG. 4. Vessels (a) and interstitial (b) particles distribution vs tumour radius—low uptake rate case.

The main results show that geometrical tortuosity can significantly impair heat transport within the tumour and that a higher magnetic field can be required to reach a temperature that is sufficiently high to kill tumour cells by cancer hyperthermia. We provide a detailed and more quantitative description of the results below.

8.1 *Particle transport*

The results displayed in Fig. 3 and Fig. 4 are presented in terms of the leading order concentrations in the tumour and the vessels against the non-dimensional radius within a chosen period of time of 24 hours and 96 hours, respectively.

The solution clearly shows that the nanoparticles manage to reach the tumour center and both concentration profiles are very similar at leading order. This is due to the particles' exchange between the two compartments through the vessels' wall combined with continuity of concentrations on the tumour boundary. Due to the assumption of drug delivered intravascularly via a bolus injection on the boundary,

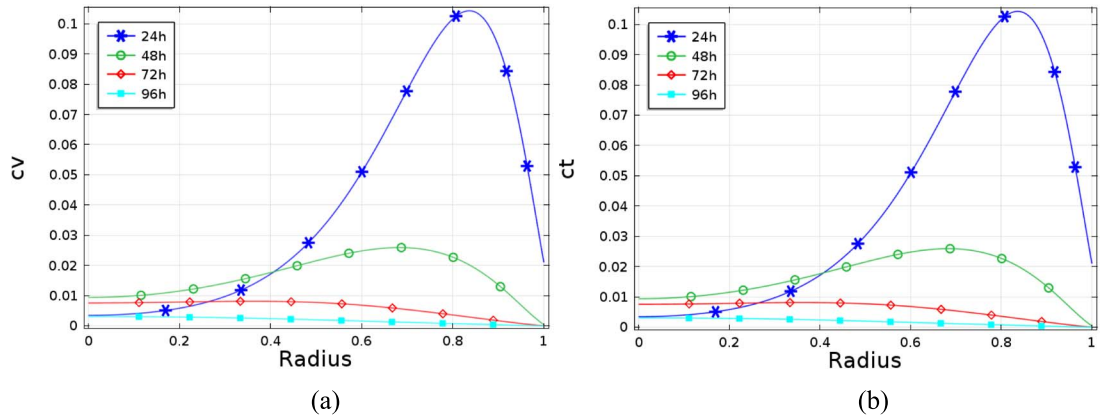

FIG. 5. Vessels (a) and interstitial (b) particles distribution vs tumour radius—high uptake rate case.

the particles' concentration decreases steadily after $6h$ (432) at $r = R$ and reaches zero after two days which cause the over all decline on the concentration. However, a fraction of the initial concentration is still able to reach the tumour centre by the end of the time interval under investigation. In the period of time $(24h - 72h)$, the particles' concentration in the center increases from 1% to approximately 7% of the initial concentration. After that, the concentration in the center starts to decrease slightly, i.e. in the period $(72h - 96h)$. In addition, the concentration in the past two days reaches a plateau when moving towards the center.

Nabil & Zunino (2016) presented their result in a cubic symmetric setting and they found that the particles' concentration decreases with time. Moreover, the concentration of nanoparticles in the vessels becomes almost uniform at the end of the circulation time they investigate, which is 48 hours.

Nanoparticles and in general drugs are eventually metabolized by tissue. This is done at a specific rate, also referred to as the *uptake* rate, which depends on the properties of the tissue and drugs at hand, as discussed by Tchoryk *et al.* (2019). Mascheroni & Penta (2017) compared two specific macromolecules characterized by different uptake rates, with order of magnitudes varying from $10^{-11}\, s^{-1}$ to $10^{-5}\, s^{-1}$, as also mentioned by Weinberg *et al.* (2007). In Fig. 5 we show the influence of high tissue uptake rate on the particle distribution in vascularised tumours, and we then increase the value of the uptake rate from $1.07 \cdot 10^{-11}\, s^{-1}$ (see Table 1) to $10^{-5}\, s^{-1}$.

The concentrations in both compartments are decreasing and approximately approaching zero at the center in all periods of time. High uptake rate leads to fast washing out the particles and few of them can reach the center of the tumour. The particles in this case are metabolized very fast by the tumour before they are transported into the tumor center.

The concentrations profiles are qualitatively in agreement with Mascheroni & Penta (2017) and this is shown for the case of the most tortuous vessels' network considered by Penta & Ambrosi (2015) and Mascheroni & Penta (2017), i.e. $\omega = 3$ and $A = r_c$, see also Table 2 and Fig. 8.

8.2 *Heat transport*

We now present the major results obtained by solving the full system of macro-scale coupled PDEs (7.1)–(7.2) by finite elements. The tortuosity of the microstructure is varied according to the

TABLE 2 *The computational result for the non-dimensional vessels' thermal conductivity with different vessels tortuosity from the analysis by Penta & Ambrosi (2015) and Mascheroni & Penta (2017)*

ω	A	$\lvert\Omega_v\rvert$	$\lvert\Omega_t\rvert$	S	H_v	$I - \langle\frac{\partial g_1}{\partial y_1}\rangle_v = I - \langle\frac{\partial a_1}{\partial y_1}\rangle_v$
0	0	$8.1 \cdot 10^{-2}$	6.149	2.30	$2.20 \cdot 10^{-4}$	$3.6 \cdot 10^{-1}$
1	r_c	$7.6 \cdot 10^{-2}$	6.154	2.32	$1.69 \cdot 10^{-4}$	$3.19 \cdot 10^{-1}$
2	r_c	$6.9 \cdot 10^{-2}$	6.162	2.57	$6.24 \cdot 10^{-5}$	$2.13 \cdot 10^{-1}$
3	$0.75r_c$	$6.8 \cdot 10^{-2}$	6.162	2.82	$2.02 \cdot 10^{-5}$	$1.59 \cdot 10^{-1}$
3	r_c	$6.5 \cdot 10^{-2}$	6.165	3.25	$4.89 \cdot 10^{-6}$	$0.9 \cdot 10^{-1}$

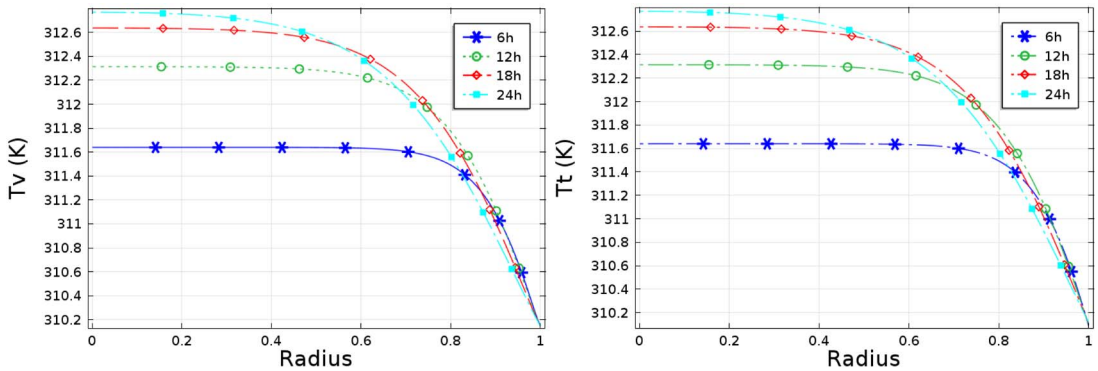

(a) (b)

FIG. 6. Temperature maps for the first 24 h in both the vessels (a) and the interstitium (b) vs radius—low uptake rate.

values reported by Penta & Ambrosi (2015) and Mascheroni & Penta (2017) corresponding to five representative geometries, and the two extreme cases are shown in Fig. 8. We have observed that the temperature increases and reaches its maximum after one day, then starts to decline and the maximum temperature varies with vessels tortuosity. As we have also remarked in the Introduction, increasing the tortuosity reduces fluid and particles convection within the tumour, as shown by Penta & Ambrosi (2015) and Mascheroni & Penta (2017). As such, this leads in turn to impaired heat convection driving a decline in temperatures. Therefore, the more regular the vessels, the lower magnetic field intensity (which is here encoded in the absorption rate coefficient) is needed to reach the desired target temperature.

The plots showing the vessels' and interstitial temperature maps are shown in Figs 6 and 7 at different times, for the first 24h and from day 1 (24h) to day 4 (96h), respectively. These results are related to the most tortuous (i.e. corresponding to the case $\omega = 3, A = r_c$ reported in Table 2) vessels' microvasculature considered by Penta & Ambrosi (2015), see Fig. 8.

Figure 6 clearly shows that the temperature increases with time as it reaches its maximum after 24 h. It then starts to decline steadily with time, because the concentration in the blood decreases exponentially according to the bolus injection, cf. initial condition (7.14).

Also, for all period of times under investigation, the temperature in the center is higher than the boundary, as the particles are transported towards the center. This can be explained by the fact that heat trasport is driven by a significant diffusive component as opposed to drug transport, which is mostly

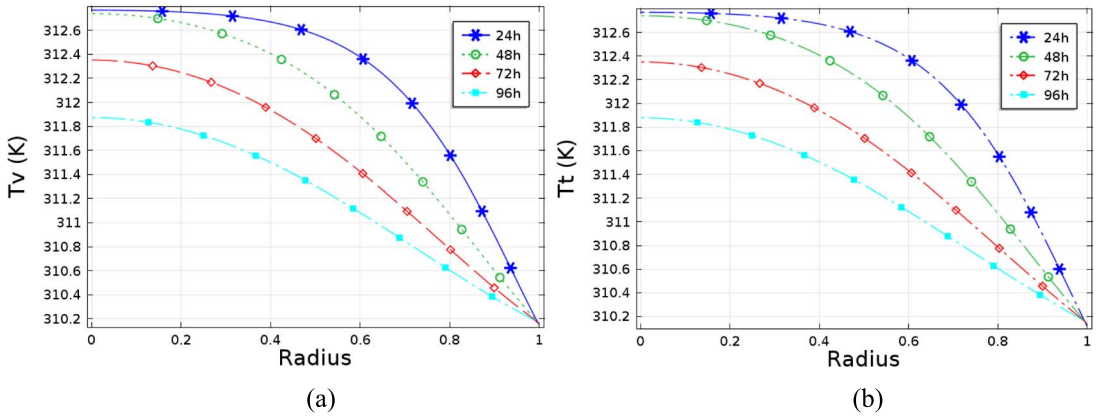

FIG. 7. Temperature maps in both the vessels (a) and the interstitium (b) vs radius—(low uptake rate) from day 1 (24h) to day 4 (96h).

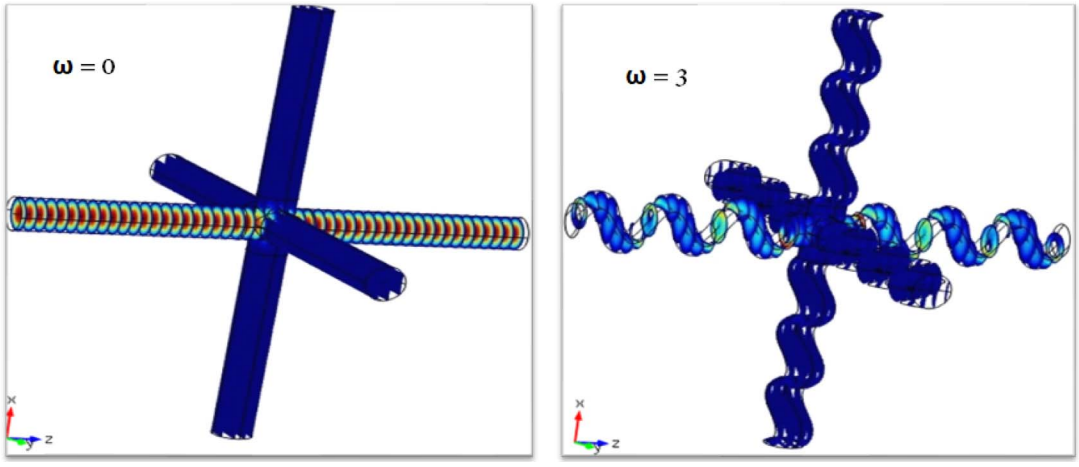

FIG. 8. The most tortuous micro-vasculature (on the right) vs the regular one (on the left) as setup by Penta & Ambrosi (2015), where further details can be found. This Figure (minimally adapted to serve this work) is reprinted from Penta & Ambrosi (2015). The role of the microvascular tortuosity in tumor transport phenomena, Journal of Theoretical Biology, 364, page 86, Fig. 4 (a) and (d), with permission from Elsevier.

driven by convection instead (cf. thermal conductivities K_t or K_v vs the particles diffusion coefficients D_v or D_t in Table 1. In fact, the non-dimensional diffusion coefficients as defined in (3.19) are of order $\approx 10^{-4}$ to 10^{-5} as opposed to the non-dimensional thermal conductivities that are of the order of $\approx 10^{-1}$ to unity). This explains the difference between the drug concentration and temperature profiles, despite both phenomena being governed by formally a similar set of advection–diffusion–reaction equations. In fact, the role of advection is more prominent in driving drug transport rather than heat transport, as it can also be observed by the more localized concentration peaks (cf. Fig. 4), as opposed to the smoother and more uniform heat transport process, which is reflected in the temperature profiles as per Figs 6 and 7. At 24 h the temperature in the center is approximately $313K$ (39.8 °C) where in the boundary it

reaches the blood temperature ($310.15K$), which is prescribed via the boundary condition. This is also in agreement with temperature profile previously reported in other works that address this problem using different modelling frameworks such as those by Bagaria & Johnson (2005); Golneshan & Lahonian (2011); Dutz & Hergt (2014).

The distribution of heat in the tumour is in agreement with Nabil & Zunino (2016) as they reported that the temperature in the center of the cube is higher than in the edges. However, Nabil & Zunino (2016) found that the temperature increases with time (48 h). This discrepancy is related to our different set of boundary conditions. In our case we have an exponential decrease in the particles' concentration, which is directly proportional to the heat source related to the magnetic absorption rate, thus eventually causing a temperature decline over time.

8.3 *The influence of absorption rate and vessels' tortuosity on the heat distribution*

The previous analyses in section 8.2 are related to tumour microvessels, which are most tortuous and leaking vessels with ($\omega = 3, A = r$) as opposed to the healthy ones ($\omega = 0$), see e.g. the works by Penta & Ambrosi (2015); Shipley & Chapman (2010) and Carmeliet & Jain (2000).

The structure of the vessels and their tortuosities are not uniform and they vary from one point to another in the tumour mass, as described by Penta *et al.* (2015). Penta & Ambrosi (2015); Mascheroni & Penta (2017) discussed the impact of the vessels' geometry on fluid and drug transport, respectively. They deduced that the vessels' tortuosity leads to a relevant decrease in both hydraulic and diffusivity properties of the vessels thus impairing fluid and drug convection within the tumour. Here, we perform a parametric analysis by varying the tortuosity of the vessels' micro-structure and capture its effect on the temperature maps. We make use of the setting that has been exploited by Penta *et al.* (2015). The data associated with the various parameters involved are reported by Penta & Ambrosi (2015); Mascheroni & Penta (2017). The results show that heat transport is impaired at increasing vessels' tortuosity from the most regular vessels characterized by $\omega = 0$ (representing healthy vessels) to the most tortuous vessels (representing tumour vessels at an advanced stage) with $\omega = 3, A = r$. The temperature varies between approximately 39.8 °C and 40.9 °C as we improve the regularity of the vessels. Also, we have observed (see Fig. 9) that the temperature decreases more remarkably from the vasculature corresponding to $\omega = 3, A = 0.75r$ and the most tortuous one ($\omega = 3, A = r$). This is ultimately related to impaired drug and fluid transport, and the latter (especially fluid convection) decreases sharply when the micro-scale fluid profile is no longer parabolic, as shown in Fig. 8 and discussed by Penta & Ambrosi (2015).

As the particles are transported smoothly in the healthy vessels and the concentration is high even in the second day, the temperature reaches its maximum 41.5 °C after two days, see Fig. 10. The difference in maximum temperatures between the regular vessels and most tortuous ones is approximately 1.5 degrees.

The temperatures achieved with different tortuosities are very close to the medical and experimental results that show that 42 °C is the appropriate temperature for hyperthermia treatment and 43 °C–44 °C for magnetic hyperthermia treatment, see also the works by Laurent *et al.* (2011); Silva *et al.* (2011); Ling-Yun *et al.* (2013).

Furthermore, the absorption rate (which is proportional to the magnetic field intensity) plays important role on the heat distribution as it mediates the temperature increase that is caused by the nanoparticles' concentration. Therefore, we have varied the value of absorption rate α at increasing tortuosity to detect the impact of these variations on temperature maps. The absorption rate of magnetic nanoparticles is proportional to the square of the magnetic field intensity, as well as its frequency. It

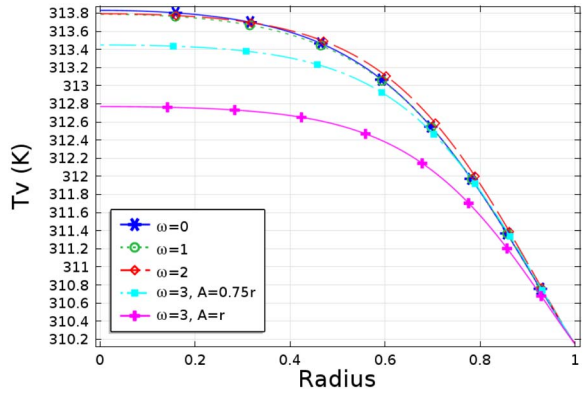

FIG. 9. The vessels' temperature vs the radius r with different vessels' structures at time 24*h*.

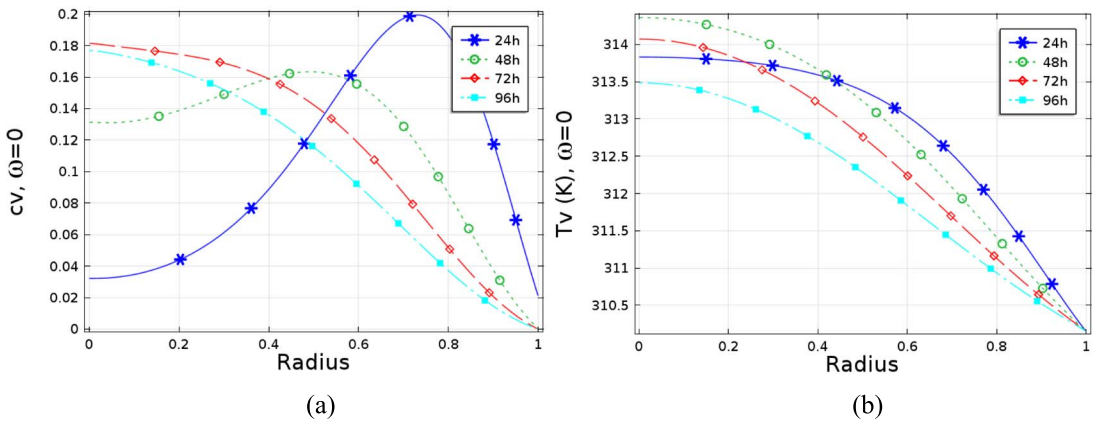

(a) (b)

FIG. 10. The vessels' concentration or temperature vs the radius r for a healthy non-tortuous microstructure.

also varies with respect to the nanoparticles size and material, and a range of variation of four orders of magnitude, i.e. from $10^3\ W/Kg$ to $10^7\ W/Kg$, has been reported by Cervadoro *et al.* (2013).

We have observed a linear relationship between the absorption rate and the heat distribution for each geometry under investigation, see Fig. 11.

Compared to the values of hydraulic conductivity, diffusivity and thermal conductivities for different vessels tortuosity, we observed that the temperature increases by 6% in the most regular vessels when the absorption rate increases by one order of magnitude. However, the temperature increases by 4.6% for the most tortuous vessels when the same change of absorption rate is applied. Moreover, when the value of the absorption rate is $6 \cdot 10^6 W/Kg$, the temperature difference between the tortuous and regular vessels is almost one degree, while the difference is approximately two degrees when the value of absorption rate is $10^7 W/kg$.

The absorption rate of nanoparticles can be varied in practice during experiments in order to have the suitable temperature that is required to kill the cancer cells.

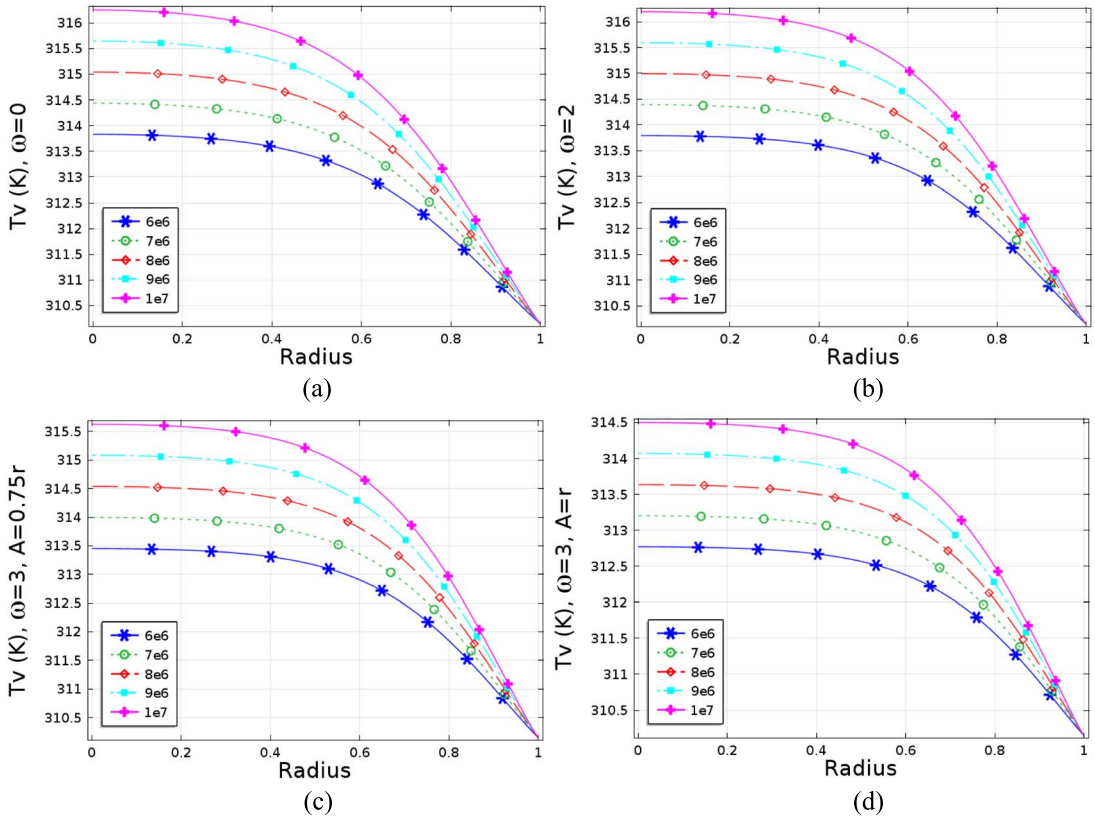

FIG. 11. Temperature maps vs normalized radius at increasing absorption rate for different microvascular geometries after 24 h.

9. Conclusion

We have derived a new mathematical model which describes the heat transport occurring in vascularised tumours due to IONPs delivered intravascularly, as per current cancer hyperthermia protocols.

We have obtained the results by means of the asymptotic homogenisation technique in terms of a tissue-scale macroscopic description of the coupling between fluid, particles and heat transport, as well as their exchange across the vessels' membranes.

The new coupled system comprises six PDEs describing both interstitial and vascular pressures, concentrations of nanoparticles, and temperatures.

A double Darcy's system describes fluid flow, while the concentration of nanoparticles and heat transport are both governed by double advection–diffusion–reaction system of PDEs.

The impact of the micro-structure is reflected in the effective tensors of coefficients representing the hydraulic and thermal conductivities, as well as particles' diffusion. These effective coefficients can be computed by solving periodic cell problems where the geometry of the micro-vessels is clearly resolved. The role of transvascular mass, heat and particles transport and uptake appears in suitable macro-scale exchange terms that provide the coupling between the governing equations in the vessels and the tumour.

We have solved the full model by means of finite elements, and we have observed that vessels' tortuosity can impair heat transport within the tumour mass, so that regularization of the micro-vessels can produce a significant (1–2 degrees) increase in the maximum temperature that is reached in the tumour center under the same therapeutic conditions (which are here reflected in the tumour absorption rate, which is in turn related to the magnetic field and nanoparticles' properties). Furthermore, we have investigated the impact of a change in the absorption rate for different micro-vessels' geometries, and this analysis can pave the way for informed cancer hyperthermia parameters depending on the geometry of the microvessels, which is ultimately related to the tumour stage. For example, the heat distribution with absorption rate 10^7 fluctuates between approximately 43.5 °C and 41.5 °C, which is aligned with the required temperature to destroy cancer cells, as mentioned in section 8.2.

This analysis is open for improvement and further developments. We have chosen to present the results by means of a spherical coordinate setting as this has enabled us to deduce the semi-analytical results that can be readily compared against the current literature. However, our finite element computational platform can be generalized to generic macro-scale geometries depending on the actual tumour shape at hand. This work could also be generalized to include nonlinear heat sources and nonlinear drug uptake, as, given the current scaling assumptions, relevant modifications would only appear at leading order. Different boundary and initial conditions could also be taken into account depending on the interplay between the tumour mass and the surrounding and on the clinical injections conditions at hand. In addition, we have derived our model by considering the same distinguished limit as in Penta *et al.* (2015); Mascheroni & Penta (2017) in terms of Peclet numbers and non-dimensional thermal hydraulic conductivities. Alternative distinguished limits, which would result in purely convective heat and drug transport contributions at leading order could be considered (see, e.g. Shipley & Chapman (2010) when these are investigated for macromolecules transport). An interesting further development of this work also resides in a comprehensive analysis of admissible distinguished limits that exist for this system, with particular reference to particles' uptake, and diffusion phenomena occurring in different regions of the domain under consideration, see, e.g. Dalwadi *et al.* (2018); Ptashnyk & Roose (2010), respectively. Furthermore, we did not consider the adhesion between the particles and the vessels' wall, and also inter-particle cohesion, which are e.g. discussed by Decuzzi & Ferrari (2006); Nabil & Zunino (2016). Whenever the adhesion mechanism is primarily driving heat transport (i.e. when the nanoparticles' dimensions prevent them from extravasating into the tumour), the dynamics of the problem changes, but can be as well investigated by means of upscaling techniques such as the asymptotic homogenisation. As such, our results can indeed also provide a basis for future research concerning different transport mechanisms, which will be investigated in future works.

Moreover, in this work, we have defined the transformation of the magnetic field to heat mediated by the absorption rate. The latter is actually related to the properties of the magnetic field, such as its intensity and frequency, as well as the shape and dimensions of the injected nanoparticles, as per the Brownian–Neel relaxation formula (Kaddi *et al.*, 2013; Pankhurst *et al.*, 2003).

Finally, a natural generalization of this work resides in considering the role of tumour growth and deformations (see, e.g. the theoretical works by Penta *et al.* (2014); Penta & Merodio (2017)), and the corresponding stresses that are due to this interplay, on nanoparticle delivery.

Acknowledgements

T.A. acknowledges the Ministry of higher education and innovation of Oman for the scholarship that supports this research. R.P. is partially supported by the Engineering and Physical Sciences Research Council grants EP/S030875/1 and EP/T017899/1 and conducted the research according to the inspiring

scientific principles of the national Italian mathematics association Indam ('Istituto nazionale di Alta Matematica'). The authors are grateful to Radostin Simitev for fruitful discussions concerning this work.

References

Bagaria, H. and Johnson, D. (2005). Transient solution to the bioheat equation and optimization for magnetic fluid hyperthermia treatment. *Int. J. Hyperth.*, **21**, 57–75.

Bakhvalov, N. & Panasenko, G. (1989) *Homogenization: Averaging Processes in Periodic Media*. Kluwer Academic Publishers.

Carmeliet, P. and Jain, R. K. (2000). Angiogenesis in cancer and other diseases. *Nature*, **407**, 249–257.

Cattaneo, L. and Zunino, P. (2014a). Computational models for fluid exchange between microcirculation and tissue interstitium. *Networks Heterogen. Media*, **9**, 135–159.

Cattaneo, L. and Zunino, P. (2014b). A computational model of drug delivery through microcirculation to compare different tumor treatments. *Int. J. Numer. Method. Biomed. Eng.*, **30**, 1347–1371.

Cervadoro, A., Giverso, C., Pande, R., Sarangi, S., Preziosi, L., Wosik, J., Brazdeikis, A., and Decuzzi, P. (2013). Design maps for the hyperthermic treatment of tumors with superparamagnetic nanoparticles. *PLoS One*, **8**, e57332.

Chou, C.-Y., Huang, C.-K., Lu, K.-W., Horng, T.-L., and Lin, W.-L. (2013). Investigation of the spatiotemporal responses of nanoparticles in tumor tissues with a small-scale mathematical model. *PLoS One*, **8**, e59135.

Cioranescu, D. & Donato, P. (1999) *An Introduction to Homogenization*. Oxford University Press.

Dalwadi, M. P. and King, J. (2020). A systematic upscaling of nonlinear chemical uptake within a biofilm. *SIAM J. Appl. Math.*, **80**, 1723, 1750.

Dalwadi, M. P., Wang, Y., King, J. R., and Minton, N. P. (2018). Upscaling diffusion through first-order volumetric sinks: a homogenization of bacterial nutrient uptake. *SIAM J. Appl. Math.*, **78**, 1300–1329.

Davit, Y., Bell, C. G., Byrne, H. M., Chapman, L. A., Kimpton, L. S., Lang, G. E., Leonard, K. H., Oliver, J. M., Pearson, N. C., Shipley, R. J., Waters, S. L., Whiteley, J. P., Wood, B. D. & Quintard, M. (2013) Homogenization via formal multiscale asymptotics and volume averaging: how do the two techniques compare? *Adv. Water Resour.*, **62**, 178–206.

De la Presa, P., Luengo, Y., Multigner, M., Costo, R., Morales, M., Rivero, G., and Hernando, A. (2012). Study of heating efficiency as a function of concentration, size, and applied field in γ-fe2o3 nanoparticles. *J. Phys. Chem. C*, **116**, 25602–25610.

Decuzzi, P. and Ferrari, M. (2006). The adhesive strength of non-spherical particles mediated by specific interactions. *Biomaterials*, **27**, 5307–5314.

Dutz, S. and Hergt, R. (2014). Magnetic particle hyperthermia-a promising tumour therapy? *Nanotechnology*, **25**, 452001.

Golneshan, A. and Lahonian, M. (2011). The effect of magnetic nanoparticle dispersion on temperature distribution in a spherical tissue in magnetic fluid hyperthermia using the lattice Boltzmann method. *Int. J. Hyperth.*, **27**, 266–274.

Hanahan, D. and Weinberg, R. A. (2011). Hallmarks of cancer: the next generation. *Cell*, **144**, 646–674.

Hashizume, H., Baluk, P., Morikawa, S., McLean, J. W., Thurston, G., Roberge, S., Jain, R. K., and McDonald, D. M. (2000). Openings between defective endothelial cells explain tumor vessel leakiness. *Am. J. Pathol.*, **156**, 1363–1380.

Jain, R. K. and Baxter, L. T. (1988). Mechanisms of heterogeneous distribution of monoclonal antibodies and other macromolecules in tumors: significance of elevated interstitial pressure. *Cancer Res.*, **48**, 7022–7032.

Jain, R. K., Tong, R. T., and Munn, L. L. (2007). Effect of vascular normalization by antiangiogenic therapy on interstitial hypertension, peritumor edema, and lymphatic metastasis: insights from a mathematical model. *Cancer Res.*, **67**, 2729–2735.

Kaddi, C. D., Phan, J. H., and Wang, M. D. (2013). Computational nanomedicine: modeling of nanoparticle-mediated hyperthermal cancer therapy. *Nanomedicine*, **8**, 1323–1333.

Laurent, S., Dutz, S., Häfeli, U. O., and Mahmoudi, M. (2011). Magnetic fluid hyperthermia: focus on superparamagnetic iron oxide nanoparticles. *Adv. Colloid Interf. Sci.*, **166**, 8–23.

Ling-Yun, Z., Jia-Yi, L., Wei-Wei, O., Dan-Ye, L., Li, L., Li-Ya, L., and Jin-Tian, T. (2013). Magnetic-mediated hyperthermia for cancer treatment: research progress and clinical trials. *Chin. Phys. B*, **22**, 108104.

Martinkova, P., Brtnicky, M., Kynicky, J., and Pohanka, M. (2018). Iron oxide nanoparticles: innovative tool in cancer diagnosis and therapy. *Adv. Healthc. Mater.*, **7**, 1700932.

Mascheroni, P. and Penta, R. (2017). The role of the microvascular network structure on diffusion and consumption of anticancer drugs. *Int. J. Numer. Method. Biomed. Eng.*, **33**, e2857.

Miaskowski, A. and Sawicki, B. (2013). Magnetic fluid hyperthermia modeling based on phantom measurements and realistic breast model. *IEEE Trans. Biomed. Eng.*, **60**, 1806–1813.

Nabil, M. and Zunino, P. (2016). A computational study of cancer hyperthermia based on vascular magnetic nanoconstructs. *Royal Soc. Open Sci.*, **3**, 160287.

O'Dea, R. D., Nelson, M., El Haj, A., Waters, S. L., and Byrne, H. M. (2015). A multiscale analysis of nutrient transport and biological tissue growth in vitro. *Math. Med. Biol. J. IMA*, **32**, 345–366.

Pankhurst, Q. A., Connolly, J., Jones, S. K., and Dobson, J. (2003). Applications of magnetic nanoparticles in biomedicine. *J. Phys. D Appl. Phys.*, **36**, R167, R181.

Penta, R. & Ambrosi, D. (2015) The role of the microvascular tortuosity in tumor transport phenomena. *J. Theor. Biol.*, **364**, 80–97.

Penta, R. & Gerisch, A. (2017) An introduction to asymptotic homogenization. *Multiscale Models in Mechano and Tumor Biology*. Springer, pp. 1–26.

Penta, R. and Merodio, J. (2017). Homogenised modeling for vascularised poroelastic materials. *Meccanica*, **52**, 3321–3343.

Penta, R., Ambrosi, D., and Shipley, R. (2014). Effective governing equations for poroelastic growing media. *Quart. J. Mech. Appl. Math.*, **67**, 69–91.

Penta, R., Ambrosi, D., and Quarteroni, A. (2015). Multiscale homogenization for fluid and drug transport in vascularised malignant tissues. *Math. Model. Method. Appl. Sci.*, **25**, 79–108.

Penta, R., Ramírez-Torres, A., Merodio, J., and Rodríguez-Ramos, R. (2021). Effective governing equations for heterogenous porous media subject to inhomogeneous body forces. *Math. Eng.*, **3**, 1–17.

Ptashnyk, M. and Roose, T. (2010). Derivation of a macroscopic model for transport of strongly sorbed solutes in the soil using homogenization theory. *SIAM J. Appl. Math.*, **70**, 2097–2118.

Saeedi, M., Vahidi, O., Goodarzi, V., Saeb, M. R., Izadi, L., and Mozafari, M. (2017). A new prospect in magnetic nanoparticle-based cancer therapy: taking credit from mathematical tissue-mimicking phantom brain models. *Nanomedicine*, **13**, 2405–2414.

Shipley, R. J. and Chapman, S. J. (2010). Multiscale modelling of fluid and drug transport in vascular tumours. *Bull. Math. Biol.*, **72**, 1464–1491.

Silva, A. C., Oliveira, T. R., Mamani, J. B., Malheiros, S. M., Malavolta, L., Pavon, L. F., Sibov, T. T., AmaroJr., E., Tannús, A., Vidoto, E. L., et al. (2011) Application of hyperthermia induced by superparamagnetic iron oxide nanoparticles in glioma treatment. *Int. J. Nanomed.*, **6**, 591.

Singh, M., Manikandan, S., and Kumaraguru, A. (2011). Nanoparticles: a new technology with wide applications. *Res. J. Nanosci. Nanotech.*, **1**, 1–11.

Taffetani, M., De Falco, C., Penta, R., Ambrosi, D., and Ciarletta, P. (2014). Biomechanical modelling in nanomedicine: multiscale approaches and future challenges. *Arch. Appl. Mech.*, **84**, 1627–1645.

Tang, Y.-d., Jin, T., and Flesch, R. C. (2018). Impact of different infusion rates on mass diffusion and treatment temperature field during magnetic hyperthermia. *Int. J. Heat Mass Transf.*, **124**, 639–645.

Tchoryk, A., Taresco, V., Argent, R. H., Ashford, M., Gellert, P. R., Stolnik, S., Grabowska, A., and Garnett, M. C. (2019). Penetration and uptake of nanoparticles in 3d tumor spheroids. *Bioconjug. Chem.*, **30**, 1371–1384.

Weinberg, B. D., Patel, R. B., Exner, A. A., Saidel, G. M., and Gao, J. (2007). Modeling doxorubicin transport to improve intratumoral drug delivery to rf ablated tumors. *J. Control. Release*, **124**, 11–19.

A. Appendix: the upscaled governing equations for the vessels

The multi-scale differential equations governing vessels fluid flow, particle and heat transport in the vessels can be obtained from equations 3.23.3, (3.6) and (3.8) with interface conditions (3.11), (3.10), (3.13) and (3.15). We have, by enforcing equation (4.2) and multiplying each equation by a suitable power of ε:

$$\varepsilon\nabla_y^2\mathbf{u}_v^{(\varepsilon)} + 2\varepsilon^2\nabla_y\cdot\nabla_x\mathbf{u}_v^{(\varepsilon)} + \varepsilon^3\nabla_x^2\mathbf{u}_v^{(\varepsilon)} = \varepsilon\nabla_x P_v^{(\varepsilon)} + \nabla_y P_v^{(\varepsilon)} \quad in \quad \Omega_v \tag{A.1}$$

$$\varepsilon\nabla_x\cdot\mathbf{u}_v^{(\varepsilon)} + \nabla_y\cdot\mathbf{u}_v^{(\varepsilon)} = 0 \quad in \quad \Omega_v \tag{A.2}$$

$$\begin{aligned}&\varepsilon^2\frac{\partial c_v^{(\varepsilon)}}{\partial t} + \nabla_x\cdot\left(\varepsilon^2 c_v^{(\varepsilon)}\mathbf{u}_v^{(\varepsilon)} - \varepsilon^2\bar{D}_v\nabla_x c_v^{(\varepsilon)} - \varepsilon\bar{D}_v\nabla_y c_v^{(\varepsilon)}\right) + \\ &\nabla_y\cdot\left(\varepsilon c_v^{(\varepsilon)}\mathbf{u}_v^{(\varepsilon)} - \varepsilon\bar{D}_v\nabla_x c_v^{(\varepsilon)} - \bar{D}_v\nabla_y c_v^{(\varepsilon)}\right) = 0, \quad in \quad \Omega_v\end{aligned} \tag{A.3}$$

$$\begin{aligned}&\varepsilon^2\frac{\partial T_v^{(\varepsilon)}}{\partial t} + \nabla_x\cdot\left(\varepsilon^2 T_v^{(\varepsilon)}\mathbf{u}_v^{(\varepsilon)} - \varepsilon^2\bar{K}_v\nabla_x T_v^{(\varepsilon)} - \varepsilon\bar{K}_v\nabla_y T_v^{(\varepsilon)}\right) + \\ &\nabla_y\cdot\left(\varepsilon T_v^{(0)}\mathbf{u}_v^{(\varepsilon)} - \varepsilon\bar{K}_v\nabla_x T_v^{(\varepsilon)} - \bar{K}_v\nabla_y T_v^{(\varepsilon)}\right) = \bar{\alpha}_v c_v^{(\varepsilon)} \quad in \quad \Omega_v.\end{aligned} \tag{A.4}$$

The interface conditions are:

$$\mathbf{u}_v^{(\varepsilon)}\cdot\mathbf{n} = \varepsilon\bar{L}\left(P_v^{(\varepsilon)} - P_t^{(\varepsilon)}\right) \quad on \quad \Gamma \tag{A.5}$$

$$\mathbf{u}_v^{(\varepsilon)}\cdot\tau = -\bar{\varphi}\left[(\mathbf{n}\cdot\left(\varepsilon\nabla_x + \nabla_y\right)\mathbf{u}_v^{(\varepsilon)}\right]\cdot\tau \quad on \quad \Gamma \tag{A.6}$$

$$(\varepsilon c_v^{(\varepsilon)}\mathbf{u}_v^{(\varepsilon)} - \varepsilon\bar{D}_v\nabla_x c_v^{(\varepsilon)} - \bar{D}_v\nabla_y c_v^{(\varepsilon)})\cdot\mathbf{n} = \varepsilon^2\bar{p}(c_v^{(\varepsilon)} - c_t^{(\varepsilon)}) \quad on \quad \Gamma \tag{A.7}$$

$$\left(\varepsilon T_v^{(\varepsilon)}\mathbf{u}_v^{(\varepsilon)} - \varepsilon\bar{K}_v\nabla_x T_v^{(\varepsilon)} - \bar{K}_v\nabla_y T_v^{(\varepsilon)}\right)\cdot\mathbf{n} = \varepsilon^2\bar{\beta}_v\left(T_v^{(\varepsilon)} - T_t^{(\varepsilon)}\right) \quad on \quad \Gamma. \tag{A.8}$$

We now equate the same coefficients for ascending powers of ε. For ε^0 we obtain:

$$\nabla_y P_v^{(0)} = 0 \quad in \quad \Omega_v \tag{A.9}$$

$$\nabla_y\cdot\mathbf{u}_v^{(0)} = 0 \quad in \quad \Omega_v \tag{A.10}$$

$$\mathbf{u}_v^{(0)}\cdot\mathbf{n} = 0 \quad on \quad \Gamma \tag{A.11}$$

$$\mathbf{u}_v^{(0)}\cdot\tau = -\bar{\varphi}[\mathbf{n}\cdot(\nabla_y\mathbf{u}_v^{(0)})]\cdot\tau \quad on \quad \Gamma \tag{A.12}$$

$$\nabla_y^2 c_v^{(0)} = 0 \quad in \quad \Omega_v \tag{A.13}$$

$$\left(\nabla_y c_v^{(0)}\right)\cdot\mathbf{n} = 0 \quad on \quad \Gamma \tag{A.14}$$

$$\nabla_y^2 T_v^{(0)} = 0 \quad in \quad \Omega_v \tag{A.15}$$

$$\left(\nabla_y T_v^{(0)}\right)\cdot\mathbf{n} = 0 \quad on \quad \Gamma. \tag{A.16}$$

For ε^1:

$$\nabla_y^2 \mathbf{u}_v^{(0)} = \nabla_x P_v^{(0)} + \nabla_y P_v^{(1)} \quad in \quad \Omega_v \tag{A.17}$$

$$\nabla_x \cdot \mathbf{u}_v^{(0)} + \nabla_y \cdot \mathbf{u}_v^{(1)} = 0 \quad in \quad \Omega_v \tag{A.18}$$

$$\mathbf{u}_v^{(1)} \cdot \mathbf{n} = \bar{L}\left(P_v^{(0)} - P_t^{(0)}\right) \quad on \quad \Gamma \tag{A.19}$$

$$\mathbf{u}_v^{(1)} \cdot \tau = -\bar{\varphi}\left[\mathbf{n} \cdot \left(\nabla_x \mathbf{u}_v^{(0)} + \nabla_y \mathbf{u}_v^{(1)}\right)\right] \cdot \tau \quad on \quad \Gamma \tag{A.20}$$

$$\nabla_y^2 c_v^{(1)} = 0 \quad in \quad \Omega_v \tag{A.21}$$

$$\left(\nabla_y c_v^{(1)}\right) \cdot \mathbf{n} = -\left(\nabla_x c_v^{(0)}\right) \cdot \mathbf{n} \quad on \quad \Gamma \tag{A.22}$$

$$\nabla_y^2 T_v^{(1)} = 0 \quad in \quad \Omega_v \tag{A.23}$$

$$\left(\nabla_y T_v^{(1)}\right) \cdot \mathbf{n} = -\left(\nabla_x T_v^{(0)}\right) \cdot \mathbf{n} \quad on \quad \Gamma. \tag{A.24}$$

For ε^2

$$\frac{\partial c_v^{(0)}}{\partial t} + \nabla_x \cdot \left(c_v^{(0)} \mathbf{u}_v^{(0)} - \bar{D}_v \nabla_x c_v^{(0)} - \bar{D}_v \nabla_y c_v^{(1)}\right) +$$
$$\nabla_y \cdot \left(c_v^{(1)} \mathbf{u}_v^{(0)} + c_v^{(0)} \mathbf{u}_v^{(1)} - \bar{D}_v \nabla_x c_v^{(1)} - \bar{D}_v \nabla_y c_v^{(2)}\right) = 0 \quad in \quad \Omega_v \tag{A.25}$$

$$\left(c_v^{(1)} \mathbf{u}_v^{(0)} + c_v^{(0)} \mathbf{u}_v^{(1)} - \bar{D}_v \nabla_x c_v^{(1)} - \bar{D}_v \nabla_y c_v^{(2)}\right) \cdot \mathbf{n} = \bar{p}(c_v^{(0)} - c_t^{(0)}) \quad on \quad \Gamma \tag{A.26}$$

$$\frac{\partial T_v^{(0)}}{\partial t} + \nabla_x \cdot \left(T_v^{(0)} \mathbf{u}_v^{(0)} - \bar{K}_v \nabla_x T_v^{(0)} - \bar{K}_v \nabla_y T_v^{(1)}\right) +$$
$$\nabla_y \cdot \left(T_v^{(0)} \mathbf{u}_v^{(1)} + T_v^{(1)} \mathbf{u}_v^{(0)} - \bar{K}_v \nabla_x T_v^{(1)} - \bar{K}_v \nabla_y T_v^{(2)}\right) = \bar{\alpha}_v c_v^{(0)} \quad in \quad \Omega_v \tag{A.27}$$

$$\left(T_v^{(0)} \mathbf{u}_v^{(1)} + T_v^{(1)} \mathbf{u}_v^{(0)} - \bar{K}_v \nabla_x T_v^{(1)} - \bar{K}_v \nabla_y T_v^{(2)}\right) \cdot \mathbf{n} = \bar{\beta}_v \left(T_v^{(0)} - T_t^{(0)}\right) \quad on \quad \Gamma. \tag{A.28}$$

Now, we determine the macro-scale relationships for the leading order velocity and pressure $\langle \mathbf{u}_v^{(0)} \rangle_v$ and $P_v^{(0)}$. Equation (A.9) implies:

$$P_v^{(0)} = P_v^{(0)}(\mathbf{x}, t). \tag{A.29}$$

This means that the leading order pressure in the vessels is y-constant. Equation (A.17) from the ε^1 conditions, together with (A.10), (A.11) and (A.12) from the ε^0 conditions, we obtain a Stokes' type problem for $\mathbf{u}_v^{(0)}$ and $P_v^{(1)}$, i.e.

$$\begin{cases} \nabla_y^2 \mathbf{u}_v^{(0)} = \nabla_x P_v^{(0)} + \nabla_y P_v^{(1)} \quad in \quad \Omega_v \\ \nabla_y \cdot \mathbf{u}_v^{(0)} = 0 \quad in \quad \Omega_v \\ \mathbf{u}_v^{(0)} \cdot \mathbf{n} = 0 \quad on \quad \Gamma \\ \mathbf{u}_v^{(0)} \cdot \tau = -\bar{\varphi}\left[(\mathbf{n} \cdot \nabla_y)\mathbf{u}_v^{(0)}\right] \cdot \tau \quad on \quad \Gamma. \end{cases}$$

Exploiting linearity, the solutions for $\mathbf{u}_v^{(0)}$ and $P_v^{(1)}$ can be formulated in terms of the following ansatz

$$\mathbf{u}_v^{(0)} = -\mathsf{W}(\mathbf{x},\mathbf{y})\nabla_x P_v^{(0)} \tag{A.30}$$

$$P_v^{(1)} = -\mathbf{m}(\mathbf{x},\mathbf{y})\nabla_x P_v^{(0)} + \bar{P}(\mathbf{x},t). \tag{A.31}$$

The auxiliary variables W and $\mathbf{m}$ are the solution of the Stokes' cell problem:

$$\nabla_y^2 \mathsf{W}^T = \nabla_y \mathbf{m} - I \quad in \quad \Omega_v \tag{A.32}$$

$$\nabla_y \cdot \mathsf{W}^T = 0 \quad in \quad \Omega_v \tag{A.33}$$

$$\mathsf{W}^T \cdot \mathbf{n} = 0 \quad on \quad \Gamma \tag{A.34}$$

$$\mathsf{W}^T \tau = -\bar{\varphi}[(\nabla_y \mathsf{W}^T)\mathbf{n}]\tau \quad on \quad \Gamma. \tag{A.35}$$

Integrating (A.30) over Ω_v leads to the average leading order velocity in the vessels:

$$\langle \mathbf{u}_v^{(0)} \rangle_v = -\mathsf{Y}\nabla_x P_v^{(0)}. \tag{A.36}$$

Here,

$$\mathsf{Y}_v = \langle \mathsf{W} \rangle_v = \frac{1}{|\Omega_v|}\int_{\Omega_v} W \mathrm{d}y. \tag{A.37}$$

Equation (A.36) shows that the vessels' fluid flow obeys the Darcy's law with hydraulic conductivity given by relationship (A.37).

In order to find the equation for the leading order pressure leading term $P_v^{(0)}$, we take the average of (A.18) and make use of interface condition (A.19), as well as the divergence theorem with respect to $\mathbf{y}$, as follows:

$$\langle \nabla_x \cdot \mathbf{u}_v^{(0)} \rangle_v + \langle \nabla_y \cdot \mathbf{u}_v^{(1)} \rangle_v = 0$$

$$\langle \nabla_x \cdot \mathbf{u}_v^{(0)} \rangle_v = -\frac{1}{|\Omega_v|}\int_\Gamma \mathbf{u}_v^{(1)} \cdot \mathbf{n} \, \mathrm{d}S_y$$

$$= -\frac{1}{|\Omega_v|}\int_\Gamma \bar{L}(P_v^{(0)} - P_t^{(0)}) \mathrm{d}S_y.$$

Therefore,

$$\nabla_x \cdot \langle \mathbf{u}_v^{(0)} \rangle_v = -\frac{1}{|\Omega_v|}\int_\Gamma \bar{L}(P_v^{(0)} - P_t^{(0)}) \, \mathrm{d}S_y. \tag{A.38}$$

Thus by means of (A.36),

$$\nabla_x \cdot (\mathsf{Y}\nabla_x P_v^{(0)}) = \frac{1}{|\Omega_v|}\int_\Gamma \bar{L}(P_v^{(0)} - P_t^{(0)}) \, \mathrm{d}S_y. \tag{A.39}$$

Equation (A.39) is the macro-scale governing equation for the leading order pressure $P_v^{(0)}$.

The leading order concentration $c_v^{(0)}$ can be found by using first equations (A.13) and (A.14), from which we deduce that the zero-th order concentration in the vessels depends on the macro-scale only,

i.e.

$$c_v^{(0)} = c_v^{(0)}(\mathbf{x}, t).$$

We can formulate an ansatz for the solution $c_v^{(1)}$ of problem (A.21)–(A.22) by exploiting linearity as follows

$$c_v^{(1)} = -\mathbf{a} \cdot \nabla_x c_v^{(0)} + \bar{c}(\mathbf{x}, t), \tag{A.40}$$

where $\mathbf{a}(\mathbf{x},\mathbf{y})$ is an auxiliary vector and $\bar{c}$ is an arbitrary $\mathbf{y}$-constant function. The solution (A.40) holds for true provided that:

$$\nabla_y^2 \mathbf{a} = 0 \quad in \quad \Omega_v \tag{A.41}$$

$$(\nabla_y \mathbf{a})\mathbf{n} = \mathbf{n} \quad on \quad \Gamma. \tag{A.42}$$

Integrating (A.25) and using the divergence theorem with respect to $\mathbf{y}$, and subsequently making use of interface condition (A.26) from equating the same power of ε^2 yields:

$$\frac{\partial c_v^{(0)}}{\partial t} + \nabla_x \cdot \left(c_v^{(0)} \langle \mathbf{u}_v^{(0)} \rangle_v - \bar{D}_v \nabla_x c_v^{(0)} - \bar{D}_v \langle \nabla_y c_v^{(1)} \rangle_v \right) + \frac{1}{|\Omega_v|} \int_\Gamma \bar{p}(c_v^{(0)} - c_t^{(0)}) \, \mathrm{d}S_y = 0,$$

where the additional contribution over the boundary $\partial\Omega_v \setminus \Gamma$ vanishes due to $\mathbf{y}$-periodicity.

Using the ansatz (A.40), we obtain:

$$\frac{\partial c_v^{(0)}}{\partial t} + \nabla_x \cdot \left(c_v^{(0)} \langle \mathbf{u}_v^{(0)} \rangle - \mathsf{F}_v \nabla_x c_v^{(0)} \right) + \frac{1}{|\Omega_v|} \int_\Gamma \bar{p} \left(c_v^{(0)} - c_t^{(0)} \right) \mathrm{d}S = 0, \tag{A.43}$$

where

$$\mathsf{F}_v = \bar{D}_v (I - \langle (\nabla_y \mathbf{a})^T \rangle_v) \tag{A.44}$$

is the effective diffusivity tensor in the vessels. Equation (A.43) is an advection–diffusion–reaction equation for $c_v^{(0)}$ and it describes the macro-scale drug dynamics in the vessels.

A macro-scale equation for the heat transport in the vessels can be obtained by following the same steps described above for particle transport. The solution of (A.15) and (A.16) is:

$$T_v^{(0)} = T_v^{(0)}(\mathbf{x}, t).$$

Therefore, $T_v^{(0)}$ is $\mathbf{y}$-constant.

The solution of the problem obtained by collecting (A.23) and (A.24) from the ε^1 conditions can be formulated in terms of the following ansatz for $T_v^{(1)}$:

$$T_v^{(1)} = -\mathbf{g} \cdot \nabla_x T_v^{(0)}(\mathbf{x}, t) + \bar{T}(\mathbf{x}, t),$$

where the auxiliary vector $\mathbf{g}$ is the solution of the following cell problem

$$\nabla_y^2 \mathbf{g} = 0 \quad in \quad \Omega_v \tag{A.45}$$

$$(\nabla_y \mathbf{g})\mathbf{n} = \mathbf{n} \quad on \quad \Gamma. \tag{A.46}$$

Integrating (A.27) and exploiting (A.28), and performing the same steps as equations (A.25) and (A.26) we reach the following macro-scale result

$$\frac{\partial T_v^{(0)}}{\partial t} + \nabla_x \cdot \left(T_v^{(0)} \langle \mathbf{u}_v^{(0)} \rangle - \mathsf{N}_v \nabla_x T_v^{(0)} \right) + \frac{1}{|\Omega_v|} \bar{\beta}_v \int_\Gamma \left(T_v^{(0)} - T_t^{(0)} \right) \mathrm{d}S = \bar{\alpha}_v c_v^{(0)}, \tag{A.47}$$

where

$$\mathsf{N}_v = \bar{K}_v (I - \langle (\nabla_y \mathbf{g})^T \rangle_v) \tag{A.48}$$

The differential equation (A.47) is an advection–diffusion–reaction type equation describing the behavior of the leading order temperature $T_v^{(0)}$ at the macro-scale.

B. Appendix: the upscaled governing equations in the tumour interstitium

In order to provide the macro-scale differential equations for fluid flow, particle transport and heat distribution related to the tumour interstitial compartment, we follow the same steps as in the vessels' case. The multi-scale equations (3.4), (3.5), (3.7), (3.9), with interface conditions (3.12), (3.14) and (3.16) can be expressed as:

$$\varepsilon \mathbf{u}_t^{(\varepsilon)} = -\varepsilon \bar{\kappa} \nabla_x P_t^{(\varepsilon)} - \kappa \nabla_y P_t^{(\varepsilon)} \quad in \quad \Omega_t \tag{B.1}$$

$$\varepsilon \nabla_x \cdot \mathbf{u}_t^{(\varepsilon)} + \nabla_y \cdot \mathbf{u}_t^{(\varepsilon)} = 0 \quad in \quad \Omega_t \tag{B.2}$$

$$\mathbf{u}_t^{(\varepsilon)} \cdot \mathbf{n}_t = \varepsilon \bar{L} \left(P_t^{(\varepsilon)} - P_v^{(\varepsilon)} \right) \quad on \quad \Gamma. \tag{B.3}$$

$$\begin{aligned} &\varepsilon^2 \frac{\partial c_t^{(\varepsilon)}}{\partial t} + \nabla_x \cdot \left(\varepsilon^2 c_t^{(\varepsilon)} \mathbf{u}_t^{(\varepsilon)} - \varepsilon^2 \bar{D}_t \nabla_x c_t^{(\varepsilon)} - \varepsilon \bar{D}_t \nabla_y c_t^{(\varepsilon)} \right) + \\ &\nabla_y \cdot \left(\varepsilon c_t^{(\varepsilon)} \mathbf{u}_t^{(\varepsilon)} - \varepsilon \bar{D}_t \nabla_x c_t^{(\varepsilon)} - \bar{D}_t \nabla_y c_t^{(\varepsilon)} \right) = -\varepsilon^2 \Upsilon c_t^{(\varepsilon)} \quad in \quad \Omega_t \end{aligned} \tag{B.4}$$

$$\left(\varepsilon c_t^{(\varepsilon)} \mathbf{u}_t^{(\varepsilon)} - \varepsilon \bar{D}_t \nabla_x c_t^{(\varepsilon)} - \bar{D}_t \nabla_y c_t^{(\varepsilon)} \right) \cdot \mathbf{n}_t = \varepsilon^2 \bar{p} \left(c_t^{(\varepsilon)} - c_v^{(\varepsilon)} \right) \quad on \quad \Gamma. \tag{B.5}$$

$$\begin{aligned} &\varepsilon^2 \frac{\partial T_t^{(\varepsilon)}}{\partial t} + \nabla_x \cdot \left(\varepsilon^2 T_t^{(\varepsilon)} \mathbf{u}_t^{(\varepsilon)} - \varepsilon^2 \bar{K}_t \nabla_x T_t^{(\varepsilon)} - \varepsilon \bar{K}_t \nabla_y T_t^{(\varepsilon)} \right) + \\ &\nabla_y \cdot \left(\varepsilon T_t^{(\varepsilon)} \mathbf{u}_t^{(\varepsilon)} - \varepsilon \bar{K}_t \nabla_x T_t^{(\varepsilon)} - \bar{K}_t \nabla_y T_t^{(\varepsilon)} \right) = \varepsilon^2 \bar{\alpha}_t c_t^{(\varepsilon)} \quad in \quad \Omega_v \end{aligned} \tag{B.6}$$

$$(\varepsilon T_t^{(\varepsilon)} \mathbf{u}_t^{(\varepsilon)} - \varepsilon \bar{K}_t \nabla_x T_t^{(\varepsilon)} - \bar{K}_t \nabla_y T_t^{(\varepsilon)}) \cdot \mathbf{n}_t = \varepsilon^2 \bar{\beta}_t \left(T_t^{(\varepsilon)} - T_v^{(\varepsilon)} \right) \quad on \quad \Gamma. \tag{B.7}$$

Here, $\mathbf{n}_t = -\mathbf{n}$ is the unit vector normal to the interface pointing from the interstitial compartment into the vessels' one. Equating the same coefficient of ϵ^0 we obtain

$$\nabla_y P_t^{(0)} = 0 \quad in \quad \Omega_t \tag{B.8}$$

$$\nabla_y \cdot \mathbf{u}_t^{(0)} = 0 \quad in \quad \Omega_t \tag{B.9}$$

$$\mathbf{u}_t^{(0)} \cdot \mathbf{n}_t = 0 \quad on \quad \Gamma \tag{B.10}$$

$$\nabla^2 c_t^{(0)} = 0 \quad in \quad \Omega_t \tag{B.11}$$

$$\left(\nabla_y c_t^{(0)}\right) \cdot \mathbf{n}_t = 0 \quad on \quad \Gamma \tag{B.12}$$

$$\nabla^2 T_t^{(0)} = 0 \quad in \quad \Omega_t \tag{B.13}$$

$$\left(\nabla_y T_t^{(0)}\right) \cdot \mathbf{n}_t = 0 \quad on \quad \Gamma \tag{B.14}$$

While for ε^1

$$\mathbf{u}_t^{(0)} = -\bar{\kappa}\nabla_x P_t^{(0)} - \bar{\kappa}\nabla_y P_t^{(1)} \quad in \quad \Omega_t \tag{B.15}$$

$$\nabla_x \cdot \mathbf{u}_t^{(0)} + \nabla_y \cdot \mathbf{u}_t^{(1)} = 0 \quad in \quad \Omega_t \tag{B.16}$$

$$\mathbf{u}_t^{(1)} \cdot \mathbf{n}_t = \bar{L}\left(P_t^{(0)} - P_v^{(0)}\right) \quad on \quad \Gamma \tag{B.17}$$

$$\nabla^2 c_t^{(0)} = 0 \quad in \quad \Omega_t \tag{B.18}$$

$$\left(\nabla_x c_t^{(0)}\right) \cdot \mathbf{n}_t = \left(\nabla_y c_t^{(1)}\right) \cdot \mathbf{n}_t \quad on \quad \Gamma \tag{B.19}$$

$$\nabla^2 T_t^{(0)} = 0 \quad in \quad \Omega_t \tag{B.20}$$

$$\left(\nabla_x T_t^{(0)}\right) \cdot \mathbf{n}_t = \left(\nabla_y T_t^{(1)}\right) \cdot \mathbf{n}_t \quad on \quad \Gamma \tag{B.21}$$

Finally, for ϵ^2, we have

$$\frac{\partial c_t^{(0)}}{\partial t} + \nabla_x \cdot \left(c_t^{(0)}\mathbf{u}_t^{(0)} - \bar{D}_t\nabla_x c_t^{(0)} - \bar{D}_t\nabla_y c_t^{(1)}\right) +$$
$$\nabla_y \cdot \left(c_t^{(1)}\mathbf{u}_t^{(0)} + c_t^{(0)}\mathbf{u}_t^{(1)} - \bar{D}_t\nabla_x c_t^{(1)} - \bar{D}_t\nabla_y c_t^{(2)}\right) = -\Upsilon c_t^{(0)} \quad in \quad \Omega_t \tag{B.22}$$

$$\left(c_t^{(1)}\mathbf{u}_t^{(0)} + c_t^{(0)}\mathbf{u}_t^{(1)} - \bar{D}_t\nabla_x c_t^{(1)} - \bar{D}_t\nabla_y c_t^{(2)}\right) \cdot \mathbf{n}_t = \bar{p}(c_t^{(0)} - c_v^{(0)}) \quad on \quad \Gamma \tag{B.23}$$

$$\frac{\partial T_t^{(0)}}{\partial t} + \nabla_x \cdot \left(T_t^{(0)}\mathbf{u}_t^{(0)} - \bar{K}_t\nabla_x T_t^{(0)} - \bar{K}_t\nabla_y T_t^{(1)}\right) +$$
$$\nabla_y \cdot \left(T_t^{(0)}\mathbf{u}_t^{(1)} + T_t^{(1)}\mathbf{u}_t^{(0)} - \bar{K}_t\nabla_x c_t^{(1)} - \bar{K}_t\nabla_y T_t^{(2)}\right) = \bar{\alpha}_t c_t^{(0)} \quad in \quad \Omega_t \tag{B.24}$$

$$\left(T_t^{(0)}\mathbf{u}_t^{(1)} + T_t^{(1)}\mathbf{u}_t^{(0)} - \bar{K}_v\nabla_x T_t^{(1)} - \bar{K}_t\nabla_y T_t^{(2)}\right) \cdot \mathbf{n}_t = \bar{\beta}_t(T_t^{(0)} - T_v^{(0)}) \quad on \quad \Gamma. \tag{B.25}$$

Firstly, we find the macro-scale equation of $\langle \mathbf{u}_t^{(0)} \rangle_t$ in terms of $P_t^{(0)}$. Equation (B.8) leads to:

$$P_t^{(0)} = P_t^{(0)}(\mathbf{x}, t).$$

Therefore $P_t^{(0)}$ is $\mathbf{y}$-constant. Substituting (B.15) from the ε^1 conditions into (B.9) and (B.10) obtained from the ε^0 conditions yields:

$$\nabla_y^2 P_t^{(1)} = 0 \quad in \quad \Omega_t \tag{B.26}$$

$$\nabla_y P_t^{(1)} \cdot \mathbf{n}_t = -\nabla_x P_t^{(0)} \cdot \mathbf{n}_t \quad on \quad \Gamma. \tag{B.27}$$

The solution $P_t^{(1)}$ is given by:

$$P_t^{(1)} = -\mathbf{r}(\mathbf{x}, \mathbf{y}) \cdot \nabla_x P_t^{(0)} + \bar{P}_t(\mathbf{x}, t), \tag{B.28}$$

where the auxiliary vector $\mathbf{r}$ solves the cell problem

$$\nabla_y^2 \mathbf{r} = 0 \quad in \quad \Omega_t \tag{B.29}$$

$$(\nabla_y \mathbf{r}) \cdot \mathbf{n}_t = \mathbf{n}_t \quad on \quad \Gamma. \tag{B.30}$$

Applying the average integral over Ω_t to (B.15) and substituting (B.28), leads to

$$\begin{aligned}\langle \mathbf{u}_t^{(0)} \rangle_t = -\frac{\bar{\kappa}}{|\Omega_t|} \int_{\Omega_t} \left(\nabla_x P_t^{(0)} - \nabla_y \left(\mathbf{r} \cdot \nabla_x P_t^{(0)} \right) \right) \mathrm{d}y &= -\frac{\bar{\kappa}}{|\Omega_t|} \int_{\Omega_t} \left(I - (\nabla_y \mathbf{r})^T \right) \nabla_x P_t^{(0)} \mathrm{d}y \\ &= -\bar{\kappa} \Upsilon_t \nabla_x P_t^{(0)},\end{aligned} \tag{B.31}$$

where

$$\Upsilon_t = I - \frac{1}{|\Omega_t|} \int_{\Omega_t} (\nabla_y \mathbf{r})^T \mathrm{d}y \tag{B.32}$$

Equation (B.31) shows that the macro-scale fluid flow in the tumor interstitium is also governed by Darcy's law.

The macro-scale equation governing the tumour interstitial pressure leading term P_t^0 can be found by taking the average over Ω_t and applying the divergence theorem to (B.16). Then using (B.17), we obtain:

$$\nabla_x \cdot \left(\bar{\kappa} \Upsilon_t \nabla_x P_t^{(0)} \right) = \frac{\bar{L} \left(P_t^{(0)} - P_v^{(0)} \right)}{|\Omega_t|} S, \tag{B.33}$$

where we exploited the fact that both $P_t^{(0)}$ and $P_v^{(0)}$ depend on the macro-scale only and S is the micro-scale surface of the capillaries defined by

$$S = \int_{\Gamma} \mathrm{dS}_y. \tag{B.34}$$

Secondly, we find the multi-scale differential equation for particle concentration in the interstitium. Equations (B.4) and (B.5) are formally identical to (A.3) and (A.7), when the following analogies are made:

$$\mathbf{u}_v \to \mathbf{u}_t, \quad c_v \to c_t, \quad \bar{D}_v \to \bar{D}_t, \quad \frac{\partial c_v}{\partial t} \to \frac{\partial c_t}{\partial t} + \Upsilon c_t, \quad |\Omega_v| \to |\Omega_t|, \quad \text{and} \quad \mathbf{n} \to \mathbf{n}_t = -\mathbf{n}. \tag{B.35}$$

The asymptotic homogenization procedures provides tumour interstitial macro-scale differential equation, which is similar to (A.43);

$$\frac{\partial c_t^{(0)}}{\partial t} + \nabla_x \cdot \left(c_t^{(0)} \langle \mathbf{u}_t^{(0)} \rangle_t - \mathsf{F}_t \nabla_x c_t^{(0)} \right) + \frac{S}{|\Omega_t|} \bar{p} \left(c_t^{(0)} - c_v^{(0)} \right) = -\Upsilon c_t^{(0)}, \tag{B.36}$$

where we have observed that both $c_v^{(0)}$ and $c_t^{(0)}$ depend only on the macro-scale $\mathbf{x}$. Equation (B.36) represents the macro-scale advection–diffusion–reaction describing interstitial particles' transport with effective diffusivity

$$\mathsf{F}_t = \bar{D}_t (I - \langle (\nabla_y \mathbf{b})^T \rangle_t). \tag{B.37}$$

The vector $\mathbf{b}$ solves the cell problem (A.41) and (A.42) in tumour interstitial domain, which is

$$\nabla_y^2 \mathbf{b} = 0 \quad in \quad \Omega_t \tag{B.38}$$

$$(\nabla_y \mathbf{b}) \mathbf{n}_t = \mathbf{n}_t \quad on \quad \Gamma. \tag{B.39}$$

Finally, the differential equation for the leading order temperature in the interstitial compartment can be computed by following the above steps together with the following identifications:

$$\mathbf{u}_v \to \mathbf{u}_t, \quad T_v \to T_t, \quad \bar{K}_v \to \bar{K}_t, \quad \frac{\partial T_v}{\partial t} \to \frac{\partial T_t}{\partial t} - \bar{\alpha} f(c_t), \quad |\Omega_v| \to |\Omega_t|, \quad \text{and} \quad \mathbf{n} \to \mathbf{n}_t = -\mathbf{n}. \tag{B.40}$$

Therefore, the multi-scale advection–diffusion–reaction for the leading order temperature in the interstitial compartment T_t^0 reads

$$\frac{\partial T_t^{(0)}}{\partial t} + \nabla_x \cdot \left(T_t^{(0)} \langle \mathbf{u}_t^{(0)} \rangle_t - \mathsf{N}_t \nabla_x T_t^{(0)} \right) + \frac{S}{|\Omega_t|} \bar{\beta}_t \left(T_t^{(0)} - T_v^{(0)} \right) = \bar{\alpha}_t c_t^{(0)}, \tag{B.41}$$

with

$$\mathsf{N}_t = \bar{K}_t (I - \langle (\nabla_y \mathbf{e})^T \rangle_t). \tag{B.42}$$

The vector $\mathbf{e}$ solves the cell problem given by (A.45) and (A.46), but in the interstitial cell portion, i.e.

$$\nabla_y^2 \mathbf{e} = 0 \quad in \quad \Omega_t \tag{B.43}$$

$$(\nabla_y \mathbf{e}) \mathbf{n}_t = \mathbf{n}_t \quad on \quad \Gamma. \tag{B.44}$$